

~~Rain-on-snow response to a warmer Pyrenees~~
Rain-on-snow responses to a warmer Pyrenees: a sensitivity analysis
using a physically-based hydrological model

Con formato: Centrado

Josep Bonsoms¹, Juan I. López-Moreno², Esteban Alonso-González³, César Deschamps-Berger², Marc Oliva¹

¹ Department of Geography, Universitat de Barcelona, Barcelona, Spain

² Instituto Pirenaico de Ecología (IPE-CSIC), Campus de Aula Dei, Zaragoza, Spain

³ Centre d'Etudes Spatiales de la Biosphère (CESBIO), Université de Toulouse, CNES/CNRS/IRD/UPS, Toulouse, France.

Corresponding author: Juan I. López-Moreno (nlopez@ipe.csic.es)

Abstract. Climate warming is changing the magnitude, timing, and spatial patterns of mountain snowpacks. A warmer atmosphere may also lead to precipitation phase shifts, with decreased snowfall fraction (Sf). The combination of Sf and snowpack decreases directly affects the frequency and intensity of rain-on-snow (ROS) events, a common cause of flash-flood events in snow dominated regions. In this work we examine the ROS patterns and sensitivity to temperature and precipitation change ~~(delta change)~~ in the Pyrenees ~~using a modelling through a~~ physical-based snow model forced with reanalysis climate data perturbed following 21st century climate projections for this mountain range. ROS patterns are characterized by their frequency, rainfall quantity and snow ablation. The highest ~~ROS fr~~ROS frequency for the baseline climate period (1980 – 2019) are found in South-West high-elevations sectors of the Pyrenees (17 days/year). Maximum ~~ROS rain~~ROS rainfall amount is detected in South-East mid-elevations areas (45 mm/day, autumn), whereas the highest ROS ablation is found in North-West high-elevations zones (- 10 cm/day, summer). When air temperature is increased from 1°C to 4°C ~~with respect to the baseline climate period,~~ ~~ROS rain~~ROS rainfall amount and frequency increase at a constant rate during winter and early spring for all elevation zones~~ss~~. For the rest of the seasons, non-linear responses of the ~~ROS fr~~ROS frequency~~equency~~ and ablation to warming are found. Overall, ~~ROS fr~~ROS frequency~~equency~~ decreases in the shoulders of the season across eastern low-elevated zones due to snow cover depletion. However, ROS increases in cold, high-elevated zones where long-lasting snow cover exists until late spring. Similarly, warming triggers fast ROS ablation (+ 10% per °C) during the coldest months of the season, high-elevations, and northern sectors where the deepest snow depths are found. On the contrary, ~~slow, and non changes in~~small differences in ROS ablation are ~~expected found~~ for warm and marginal snowpacks. These results highlight the different ROS responses to warming across the mountain range, suggest similar ROS sensitivities in near mid-latitude zones, and will help anticipate future ROS impacts in hydrological, environmental, and socioeconomic mountain systems.

Keywords: Snow, Rain-on-snow, Climate warming, Snow sensitivity, Mountain snowpack, Pyrenees.

25

26 **1 Introduction**

27

28 Mountain snowpacks supply large hydrological resources to the lowlands (García-Ruiz et al., 2015; Viviroli et
 29 al., 2011), with important implications in the ecological (Wipf and Rixen, 2010), hydrological (Barnett, 2005;
 30 Immerzeel et al., 2020) and socioeconomic systems by providing hydroelectricity (Beniston et al., 2018) or
 31 guaranteeing winter tourism activities (Spandre et al., 2019). Climate warming, however, is modifying
 32 mountain snowfall patterns (IPCC, 2022), through temperature-induced precipitation changes from snowfall
 33 to rainfall (Lynn et al., 2020), leading in some cases to rain-on-snow (ROS) events ~~in snow covered areas.~~
 34 The upward high-latitude temperature and precipitation trends (Bintanja and Andry, 2017) and ~~mountain~~
 35 ~~elevation-dependent~~ warming ~~in mountain regions~~ (Pepin et al., 2022) will likely change future ~~ROS frequency~~
 36 ~~ROS frequency (ROS fr)~~ in snow-dominated ~~areas~~ ~~regions~~ (López-Moreno et al., 2021). To date, research has
 37 been focused on the ROS predictability (Corripio and López-Moreno, 2017), detection and validation methods
 38 through remote sensing (Bartsch et al., 2010) and models (Serreze et al., 2021). Several works have examined
 39 ~~ROS fr~~ ~~ROS frequency fr~~ from the climatological point of view, by analyzing ROS spatial-temporal patterns for
 40 Alaska (Crawford et al., 2020), Japan (Ohba and Kawase, 2020), Norway (Pall et al., 2019; Mooney and Li,
 41 2021) or the Iberian Peninsula mountains (Morán-Tejeda et al., 2019). ROS events have also been linked with
 42 Northern-Hemisphere and Arctic low-frequency climate modes of variability (Rennert et al., 2009; Cohen et
 43 al., 2015) as well as synoptic weather types (Ohba and Kawase, 2020). Further, several works in mountain
 44 catchments of Switzerland (Würzer et al., 2016), Germany (Garvelmann et al., 2014a), United-States (Marks
 45 et al., 1992), Canadian Rockies (Pomeroy et al., 2016) or Spain (Corripio and López-Moreno, 2017), have
 46 portioned the contribution of Surface Energy Balance (SEB) components during ROS events. ROS alters snow
 47 and soil conditions, since the liquid water percolation creates ice layers and could alter the snowpack stability
 48 (Rennert et al., 2009). In severe ROS events, water percolation reaches the ground, and the subsequent water
 49 freezing causes latent heat releases, leading to soil and permafrost warming (Westermann et al., 2011). Positive
 50 heat fluxes during ROS events enhance snow runoff (Corripio and López-Moreno, 2017), especially in warm
 51 and wet snowpacks (Würzer et al., 2016). ROS can also trigger a snow avalanche in mountain zones (Conway
 52 and Raymond, 1993), flash flood events (Surfleet and Tullos, 2013), impacts in tundra ecosystems (Hansen et
 53 al., 2013) and herbivore populations such as reindeers (Kohler and Aanes, 2004).

54

55 Different ~~ROS frequency~~ ~~ROS fr~~ trends have been found since the last half of the 20st century. In the western
 56 United-States and from 1949 to 2003 (McCabe et al., 2007) found a general ~~ROS fr~~ ~~ROS frequency~~ decrease in
 57 ~~low- 1500 m elevations~~ but an increase in high elevations. Similarly, the analysis of six major German basins
 58 from 1990 to 2011, reveals an upward (downward) ~~ROS fr~~ ~~ROS frequency~~ trend during winter (spring) at ~~low~~
 59 ~~1500 m~~ and high elevations (Freudiger et al., 2014). On the contrary, from 1979 to 2014, no winter ~~ROS fr~~ ~~ROS~~
 60 ~~frequency~~ trends were found across the entire Northern-Hemisphere (Cohen et al., 2015). ROS projections for
 61 the end of the 21st century suggest a general ~~ROS fr~~ ~~ROS frequency~~ increase in cold regions. This is projected
 62 for Alaska (Bieniek et al., 2018), Norway (Mooney and Li, 2021), western United-States (Musselman et al.,

2018), Canada (Jeong and Sushama, 2018) or Japan (Ohba and Kawase, 2020). In European mid-latitude mountain ranges, such as the Alps, ~~ROS- \mathbf{f} ROS frequency~~ is expected to increase (decrease) in high (low) elevation sectors (Beniston and Stoffel, 2016; Morán-Tejeda et al., 2016). López-Moreno et al. (2021) compared the ROS sensitivity to climate warming across 40 global basins and detected the highest ~~ROS- \mathbf{f} ROS frequency~~ decreases in low-elevated and warm Mediterranean mountain sites. Despite the increasing understanding of ROS spatio-temporal past and future trends, little is known about the ROS sensitivity to climate warming across southern European mountain ranges, such as the Pyrenees.

~~This work examines~~Here we examine the ROS sensitivity to temperature and precipitation change (~~delta-change~~) for low (1500 m), mid (1800 m) and high (2400 m) elevations of the Pyrenees. ROS ~~delta-change~~responses to temperature and precipitation is analyzed using a physically based snow model, forced with reanalysis climate data perturbed according to 21st century climate projections spread for range (Amblar-Francés et al., 2020). Previous studies in alpine zones have shown different ROS response to warming depending on the area and month of the season (e.g., Morán-Tejeda et al. 2016). For this reason, results are focused on these two factors. First, we analyze height of snow (HS) and snowfall fraction (Sf) ~~responses to temperature and precipitation since these are the main drivers of ROS~~ (López-Moreno et al., 2021), ~~sensitivity to temperature and precipitation~~. Next, we examine ROS patterns and their response to warming by three key ROS indicators, namely:

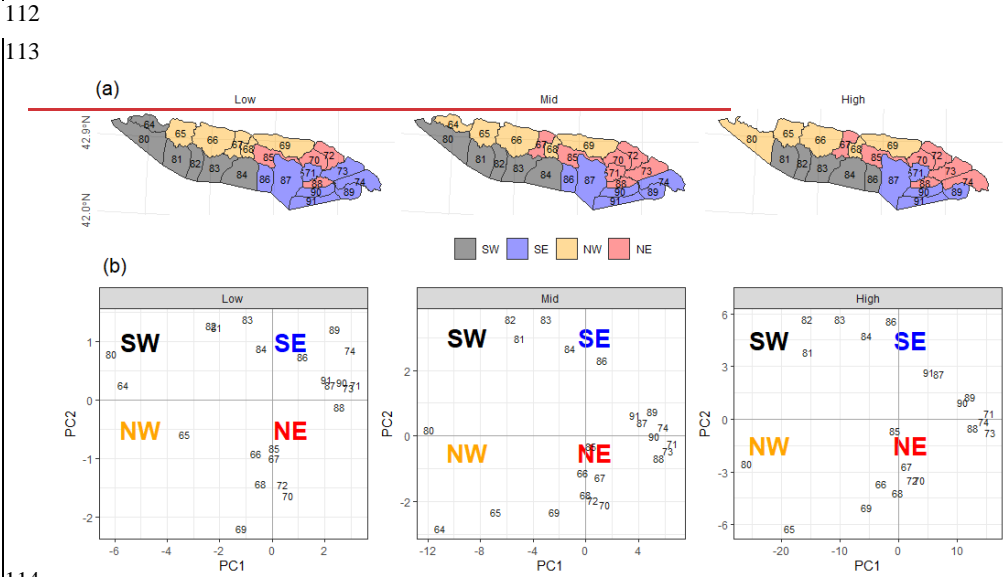
- (a) Number of ROS days for a season (~~ROS- \mathbf{f} ROS frequency~~).
- (b) Average rainfall quantity during a ROS day (~~ROS-rain~~ROS rainfall amount).
- (c) Average daily snow ablation during a ROS day (ROS ablation).

The study area is presented in Section 2. Section 3 describes the data and methods. Section 4 presents the results. We finally discuss the anticipated ROS spatio-temporal changes, their socio-environmental impacts and hazards in Section 5.

2 Regional setting

The Pyrenees mountain range is located between the Atlantic Ocean (West) and the Mediterranean Sea (East), and is the largest (~ 450 km) mountain range of the Iberian Peninsula. Elevation increases towards the central massifs, where the highest peak is found (Aneto, 3,404 m asl). Glaciers expanded during the Little Ice Age and nowadays are located in the highest mountain summits (Vidaller et al., 2021). The regional annual 0 °C isotherm is at ca. 2700 m (Del Barrio et al., 1990), and at ca. 1600 m during the cold season (López-Moreno and Vicente-Serrano, 2011). The elevation lapse-rate is ca. 0.6°/100 m, being slightly lower during winter (Navarro-Serrano and López-Moreno, 2017). Annual precipitation is ca. 1000 mm/year (ca. 1500 m); maximum values are found in the northern-western massifs (around 2000 mm/year), decreasing towards the southern-eastern (SE) area (Lemus-Canovas et al., 2019). Precipitation is predominantly (> 90%) solid above

101 1600 m from November to May (López-Moreno, 2005). Due to the mountain alignment, relief configuration,
102 and the distance to the Atlantic Ocean, seasonal snow accumulations in the northern slopes (ca. 500 cm/season),
103 almost doubles the recorded in the SE area for the same elevation (ca. 2000 m) (Bonsoms et al., 2021b). In the
104 western and central area of the southern slopes of the range (SW sector, Figure 1), snow accumulation is ruled
105 by Atlantic wet and mild flows, which are linked with negative North Atlantic Oscillation (NAO) phases (SW
106 and W synoptic weather types) (López-Moreno, 2005; Alonso-González et al., 2020b; Bonsoms et al., 2021a).
107 Positive Western Mediterranean Oscillation (WeMO) phases (NW and NE synoptic weather types) control the
108 snow patterns in the northern-eastern (NE) slopes of the range (Bonsoms et al., 2021a). Generally, snow
109 ablation starts in February (May) in low-low elevations and in May at high elevation (high) elevations. The
110 energy available for snow ablation is controlled by net radiation (55 %, over the total), latent (32 %) and
111 sensible (13 %) heat fluxes (Bonsoms et al., 2022a).



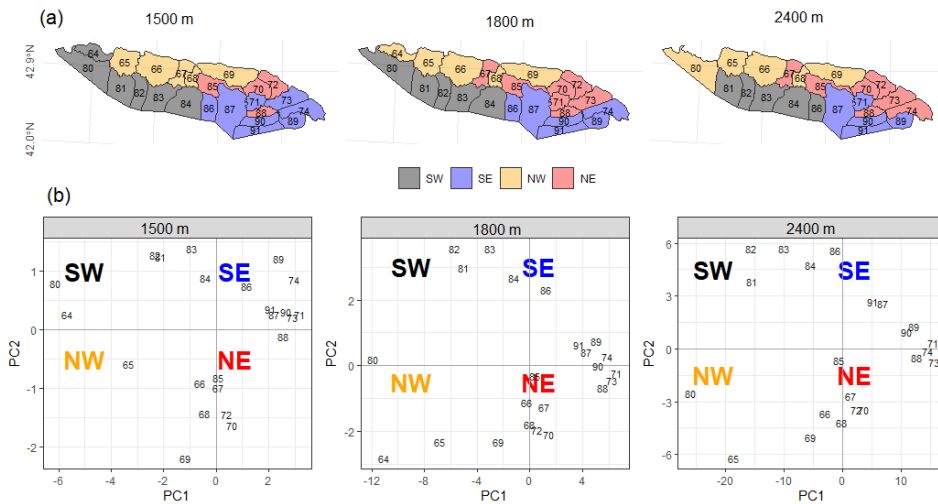


Figure 1. (a) Pyrenean massifs sectors (colors) for 1500 m low, mid- 1800 m and high-2400 m elevation. (b) Principle Component Analysis (PCA) scores of each massif for 1500 m low, mid- 1800 m and 2400 m high elevation. The black numbers are the SAFRAN massif's identity numbers defined by Vernay et al. (2022).

Note that high elevation does not include massif number 64 since this massif does not reach 2400 m.

3 Data and methods

3.1 Snow model description

Snowpack is modeled using the energy and mass balance snow model FSM2 (Essery, 2015). The FSM2 was forced at hourly resolution for each massif and elevation range (c.f. Sect. 3.3) for the baseline climate (1980 – 2019) according to and several climate perturbed climate projections scenarios (c.f. Sect. 3.4). Sf was quantified using a threshold-approach. Precipitation was snowfall when temperature was $< 1^{\circ}\text{C}$ according to previous ROS research in the study zone (Corripio and López-Moreno, 2017) and the average rain-snow temperature threshold for the Pyrenees (Jennings et al., 2018). Snow cover is calculated by a linear function of snow depth, snow albedo is estimated based on a prognostic function with the new snowfall. Snow thermal conductivity is estimated based on snow density. Liquid water percolation is calculated based on a gravitational drainage. Compaction rate is simulated from overburden and thermal metamorphism. The atmospheric stability is estimated through the Richardson number stability functions to simulate latent and sensible heat fluxes. The selected FSM2 configuration includes three snow layers and four soil layers. The detailed FSM2 physical parameters and Fortran compilation numbers are shown in Table S1. The FSM2 model and configuration was previously validated in the Pyrenees at Bonsoms et al. (2023~~2b~~). FSM2 has been successfully used in snow model sensitivity studies in alpine zones (Günther et al., 2019). FSM2 has been implemented in a wide range of alpine conditions, such as for the Iberian Peninsula mountains (Alonso-González et al., 2019), Spanish

140 Sierra Nevada (Collados-Lara et al., 2020) or swiss forest environments (Mazzotti et al., 2020) snowpack
141 modeling. FMS2 has been integrated in snow data-assimilation schemes in combination with in-situ (Smyth et
142 al., 2022) and remote-sensing data (Alonso-González et al., 2022).

143

144 3.2 Atmospheric forcing data

145

146 The FSM2 was forced with the SAFRAN meteorological system reanalysis dataset for flat ~~slopes-terrain~~
147 (Vernay et al., 2022). The SAFRAN meteorological system integrates meteorological simulations, remote-
148 sensing cloud cover data, and instrumental records through data-assimilation. SAFRAN is forced with a
149 combination of ~~homogenized~~-ERA-40 reanalysis (1958 to 2002) and the numerical weather prediction model
150 ARPEGE (2002 to 2020). SAFRAN system was firstly designed for avalanche monitoring (Durand et al.,
151 1999, 2009), but the accurate results obtained enhanced the diffusion of the meteorological system and its
152 integration in the French hydrometeorological modelling system by the local weather service, Météo-France
153 (Habets et al., 2008). SAFRAN ~~performance~~ has been extensively validated. ~~For instance, in long-term and~~
154 ~~high resolution climate analysis (Devers et al., 2021), seasonal forecasting (Ceron et al., 2010) or the~~
155 ~~meteorological modelling of continental France (Quintana Seguí et al., 2008) and Spain (Quintana Seguí et~~
156 ~~al., 2017). SAFRAN system has been used~~ as meteorological forcing data for the snow modeling in complex
157 alpine terrain (Revuelto et al., 2018; Deschamps-Berger et al., 2022), to study long-term snow evolution
158 (Réveillet et al., 2022), avalanche hazard forecasting (Morin et al., 2020), snow climate projections (Verfaillie
159 et al., 2018), snow depth (López-Moreno et al., 2020) and energy heat fluxes spatio-temporal trends (Bonsoms
160 et al., 2022a). ~~SAFRAN meteorological system exhibit an accuracy of around 1 °C in air temperature and~~
161 ~~around 20 mm in the monthly cumulative precipitation (Vernay et al., 2022).~~

162

163 3.3 Spatial areas

164

165 SAFRAN system provides data at hourly resolution from 0 to 3600 m, by steps of 300 m, grouped by massifs.
166 The SAFRAN massifs (polygons of Figure 1) were chosen for their relative topographical and climatological
167 similarities (Durand et al., 1999). We selected the 1500 m (low), 1800 m (mid), and 2400 m (high) specific
168 elevation bands of the Pyrenees. In order to retain the main spatial differences across the mountain range,
169 reduce data dimensionality and include the maximum variance, massifs with similar interannual snow
170 characteristics were grouped into sectors by performing a Principal Component Analysis (PCA). PCA is an
171 extensively applied statistical method for climatological and snow spatial regionalization (i.e., López-Moreno
172 and Vicente-Serrano, 2007; Schöner et al., 2019; Alonso-González et al., 2020a; Matiu et al., 2021; Bonsoms
173 et al., 2022a). A PCA was applied over HS data for all months and years of the baseline climate. Massifs were
174 grouped into four groups depending on the maximum correlation to the first (PC1) and second (PC2) scores.
175 Pyrenean sectors were named South-West (SW), South-East (SE), North-West (NW) and North-East (NE) due
176 to their geographical position. Figure 1 shows the resulting Pyrenean regionalization for ~~1500 m low, mid 1800~~
177 ~~m~~ and high elevation as well as the SAFRAN massifs PC1 and PC2.

178

179 **3.4 Sensitivity analysis**

180

181 ROS season extension was defined according to ROS occurrence during the baseline climate period. For the

182 purposes of this research, seasons are classified as follows: October and November (Autumn); December,

183 January, and February (Winter); March, April, May, and June (Spring); and July (Summer). August and

184 September are not included due to the absence of regular snow cover. ROS sensitivity to precipitation, ~~air~~

185 ~~temperature~~ T_a , increasing incoming longwave radiation (L_{win}) accordingly, ~~was performed though a delta-~~

186 ~~change approach~~. This method has been successfully applied and validated for analyzing the snow sensitivity

187 to temperature and precipitation changes in many mountains, such as the Pyrenees (e.g., López-Moreno et al.,

188 2013), the Iberian-Peninsula mountain areas outside the Pyrenees (Alonso-González et al., 2020a), Alps (Marty

189 et al., 2017), Canadian basins (Pomeroy et al., 2015; Rasouli et al., 2019), or western United-States

190 (Musselman et al., 2017b), among other works. ~~Delta change~~ This methodology has also been also performed

191 in global ROS sensitivity to temperature change studies (López-Moreno et al., 2021). SAFRAN reanalysis

192 climate data was perturbed according to Spanish Meteorological Agency climate change scenarios projected

193 for the 21st Century in the Pyrenees (Amblar-Francés et al., 2020). Precipitation was increased (+10%), left

194 unchanged (0 %) and decreased (- 10%). ~~Air temperature~~ T_a (°C) was perturbed from +1°C to +4°C by +1°C.

195 L_{win} was increased due to warming, by applying the Stefan-Boltzmann law, using the ~~Stefan-Boltzmann~~

196 ~~constant~~ Stefan-Boltzmann constant (σ ; $5.670373 \times 10^{-8} W m^{-2} K^{-4}$), and the hourly atmospheric emissivity

197 (ϵ_t), derived from SAFRAN T_a air temperature and L_{win} :

$$\epsilon_t = \frac{L_{win}}{\sigma (T_a + 273.15)^4}$$

201 ~~A temperature increase of 1°C can be interpreted as an optimistic projection for the region, while 2°C and 4°C~~

202 ~~would represent projections for mid and high emission scenarios, respectively (Pons et al., 2015). The range~~

203 ~~of +/-10% for precipitation includes the expected changes in precipitation according to the vast majority of~~

204 ~~climate models, regardless of the emission scenario (López-Moreno et al., 2008; Pons et al., 2015; Amblar-~~

205 ~~Francés et al., 2020).~~

207 3.5 ROS definition and HS, Sf and ROS climate indicators

208

209 The average HS and Sf ~~delta change~~ sensitivity to temperature and precipitation (expressed in % per °C) is the

210 average seasonal HS and Sf anomalies under the baseline climate and divided by degree of warming. Days are

211 classified as ROS days when daily rainfall amount was ≥ 10 mm and HS ≥ 0.1 m, according to previous

212 works (Musselman et al., 2018; López-Moreno et al., 2021). ~~ROS fr~~ ROS frequency are the number of ROS

213 days. ~~ROS rain~~ ROS rainfall amount is the average daily rainfall (mm) during a ROS day. ROS ablation is the

214 average daily snow ablation (cm) during a ROS day. The average daily snow ablation is the daily average HS

Con formato: Fuente: 11 pto

Con formato: Fuente: 11 pto

Con formato: Fuente: 11 pto

Con formato: Fuente: 11 pto

Con formato: Fuente: 11 pto

Con formato: Fuente: 11 pto

Con formato: Fuente: 11 pto

Con formato: Fuente: 11 pto

Con formato: Fuente: 11 pto

Con formato: Fuente: 11 pto

Con formato: Fuente: 11 pto

Con formato: Fuente: 11 pto

Con formato: Fuente: 11 pto

Con formato: Fuente: 11 pto

Con formato: Fuente: 11 pto

Con formato: Fuente: 11 pto

Con formato: Fuente: 11 pto

Con formato: Fuente: 11 pto

Con formato: Fuente: 11 pto

Con formato: Fuente: 11 pto

Con formato: Fuente: 11 pto

Con formato: Fuente: 11 pto

215 difference between two consecutive days (Musselman et al., 2017a). Only the days when a negative HS
216 difference occurred were selected. ROS exposure is the relation between ~~ROS-rain~~ROS rainfall amount (y-axis)
217 and ~~ROS-#~~ROS frequency (x-axis) differences from the baseline climate scenario for the massifs were ~~ROS~~
218 ~~#ROS frequency~~ is recorded for all increments of temperature.

219

220 4 Results

221

222 We provide an analysis of ROS drivers, near-present ROS patterns and their response to warming. ROS spatio-
223 temporal dynamics are analyzed by frequency, rainfall quantity and snow ablation. Since we have detected a
224 non-linear and counter-intuitive ROS sensitivity to temperature, ROS indicators values are shown for each
225 increment of temperature, grouped by elevation and sectors, namely SW, SE, NW and NE.

226

227 4.1 ~~ROS drivers~~HS and Sf response to temperature and precipitation change

228

229 HS and Sf ~~delta-change~~response to temperature and precipitation is shown in Figure 22. Seasonal HS and Sf
230 ~~delta-change~~variability is mostly controlled by the increment of temperature, season, elevation, and spatial
231 sector (~~Figure S1~~). The role of precipitation variability in the seasonal HS evolution is moderate to ~~low~~ ~~1500~~
232 ~~m~~ (Figure S12 to S34). Only in ~~high~~ ~~2400 m~~ elevation an upward trend of precipitation (at least > 10%) can
233 counterbalance small increments of temperature (< 1°C, over the baseline climate) from December to February
234 (Figure S34). For this reason, precipitation was excluded to further analysis. Snow in ~~low~~ ~~1500 m~~ and ~~mid~~
235 ~~1800 m~~ elevations during summer is rarely observed, however, marginal snow cover in ~~high~~ ~~2400 m~~ elevation
236 can last until June and July, especially in the wettest sectors of the range (NW and SW). Seasonal HS and Sf
237 ~~response to temperature delta-change~~ show ~~an elevation dependent pattern to warming and~~ large seasonality.
238 The average HS decrease per °C ranges from 39 %, 37 % and 28 % per °C, for ~~1500 m~~ ~~low~~, ~~mid~~ ~~1800 m~~ and
239 ~~high~~ ~~2400 m~~ elevations, respectively. However, relevant differences are found depending on the season and
240 degree of warming (Figure 32). Maximum HS and Sf reductions are found in ~~low~~ ~~1500 m~~ and ~~mid~~ ~~1800 m~~
241 elevations during the shoulders of the season (autumn and spring), coinciding with the time when ROS events
242 are more frequent for the baseline climate (Figure 3). In these elevations, maximum HS decreases (52 % over
243 the baseline climate) are modeled for spring when temperature is + 1°C. The greatest HS decreases in ~~high~~
244 ~~2400 m~~ elevation areas are modeled for summer (54 % HS decrease for 1°C). If temperature reaches maximum
245 values (+ 4 °C), seasonal HS is reduced 92 %, 89 %, and 79 % for low, ~~mid~~ ~~1800 m~~, and ~~high~~ ~~2400 m~~
246 elevations, respectively (Figure S45).

247

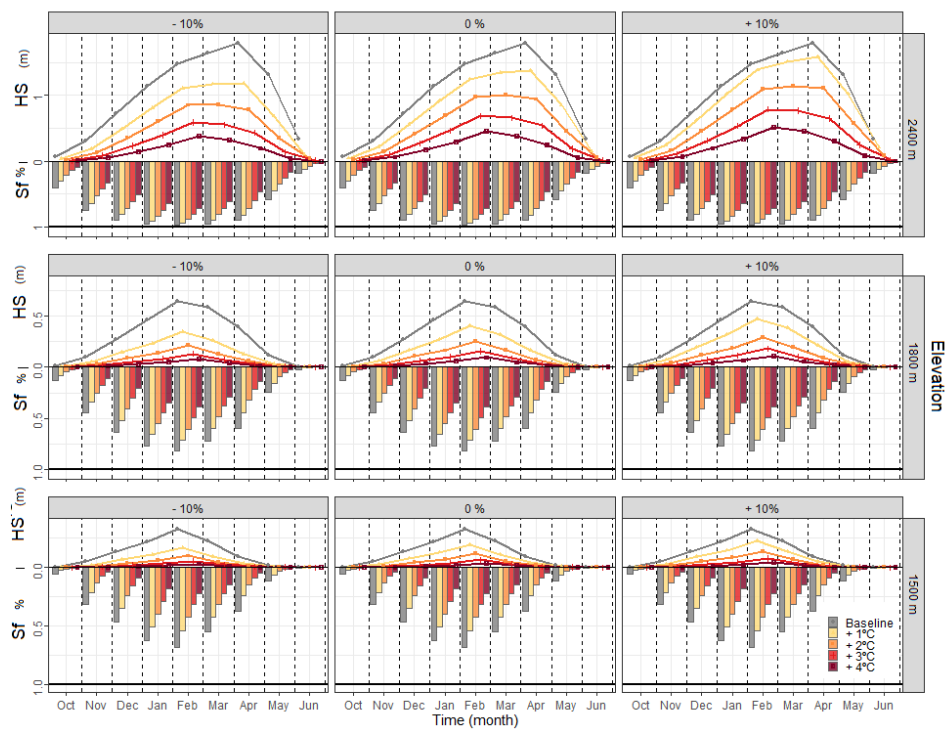
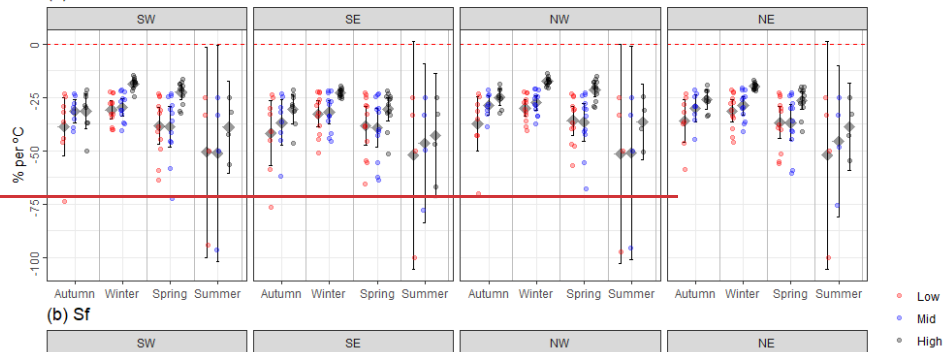


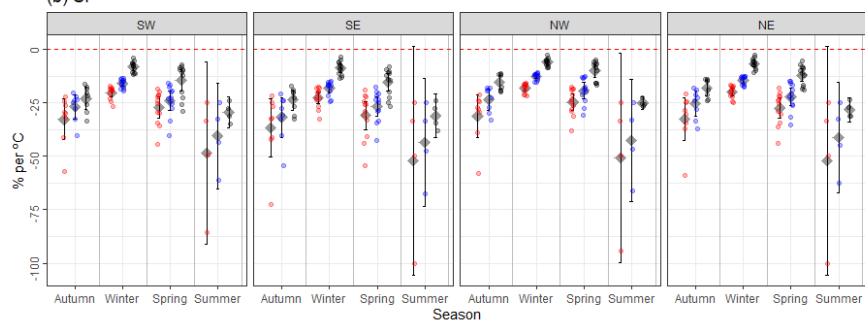
Figure 2. Height of snow (HS) (lines) and Snowfall fraction (Sf) (bars) monthly variation for baseline climate scenario and different increments of temperature (colors) grouped by elevation (rows) and sectors (columns).

253

(a) HS

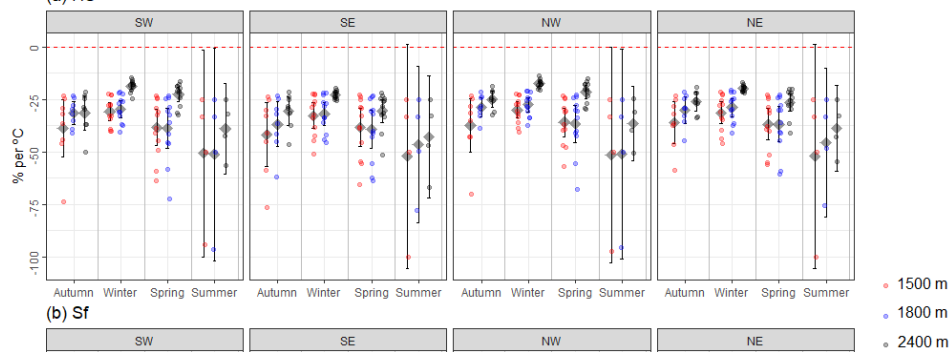


(b) Sf

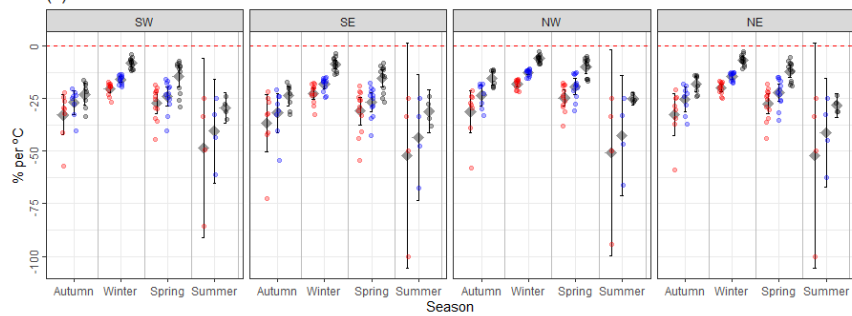


254

(a) HS



(b) Sf



255

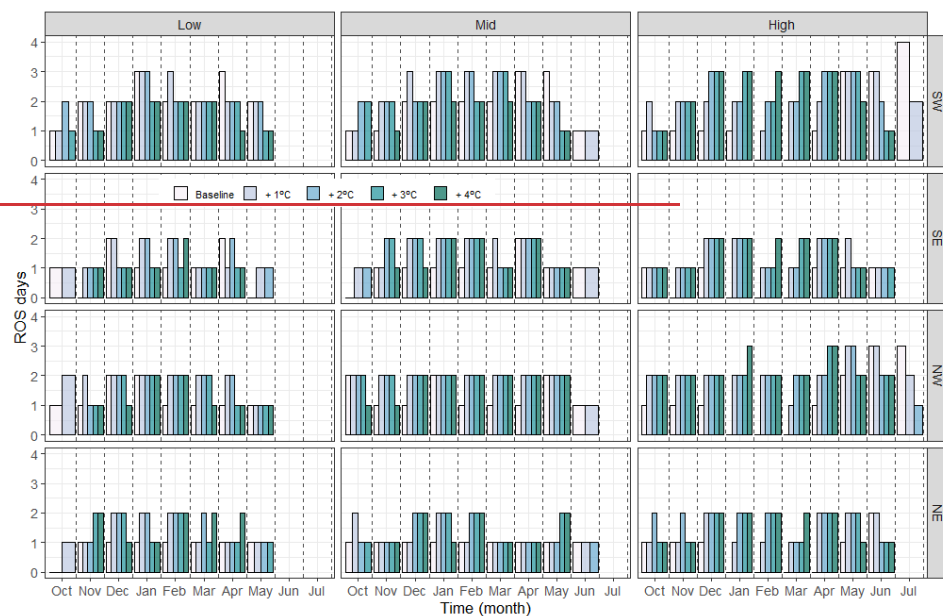
256 **Figure 32.** Seasonal (a) HS and (b) Sf anomalies over the baseline climate. Data are shown by elevation
 257 (colors), season (x-axis) and sectors (boxes). Points represent the average seasonal HS and Sf anomalies
 258 grouped by month of the season and increment of temperature (from 1°C to 4°C). The black diamond point
 259 indicates the mean, whereas the upper and lower error bars show the Gaussian confidence based on the
 260 normal distribution.

261
 262 Sf shows lower sensitivity to warming than HS and maximum reductions in autumn. On average, Sf decreases
 263 by 29%, 22 %, and 12 % per °C for low-, ~~mid- 1800 m~~, and ~~high- 2400 m~~ elevations, respectively. An increase
 264 of 4°C supposes Sf reductions of 80 %, 69 % and 49 % for low-, ~~mid- 1800 m~~, and ~~high- 2400 m~~ elevations.
 265 Different HS and Sf ~~delta-changesensitivity to temperature shows also different sensitivitiesare found~~ -across
 266 the range. Independently of the elevation band and season, the SE exhibit the greatest HS and Sf decreases
 267 (41 % and 35 % per °C, respectively). On the contrary, minimum reductions are expected in the northern slopes
 268 (NW and NE).

269 270 **4.2 ~~ROS-f~~ROS frequency**

271
 272 Low elevation annual ~~ROS-f~~ROS frequency for the baseline climate is 17, 8, 10 and 7 days/year for SW, SE,
 273 NW, NE sectors, respectively (Figure 43). The highest annual ~~ROS-f~~ROS frequency is however observed at
 274 ~~mid- 1800 m~~ elevation. Here, annual ~~ROS-f~~ROS frequency is 17, 9, 12 and 9 for SW, SE, NW, NE sectors.
 275 Within these elevations, the maximum ~~ROS-f~~ROS frequency is detected in SW during winter and spring (7
 276 days/season, for both elevations and seasons). The eastern Pyrenees follow a similar seasonality. Maximum
 277 ~~ROS-f~~ROS frequency in ~~low- 1500 m~~ elevation is found in winter (4 and 3 days/season, SE and NE,
 278 respectively), and during spring in ~~mid- 1800 m~~ elevation (4 and 3 days, SE and NE, respectively). ROS is
 279 rarely observed in SE during the latest month of spring (May), which contrast with the modeled values for SW
 280 (2 and 3 days/month, for ~~low- 1500 m~~ and ~~mid- 1800 m~~ elevations, respectively). ~~High- 2400 m~~ elevation
 281 shows the minimum ~~ROS-f~~ROS frequency. Here, comparisons between seasons reveal maximum ~~ROS-f~~ROS
 282 frequency during summer, especially in SW (7 days/season), followed by NW (6 days/season), and NE (2
 283 days/season).

285

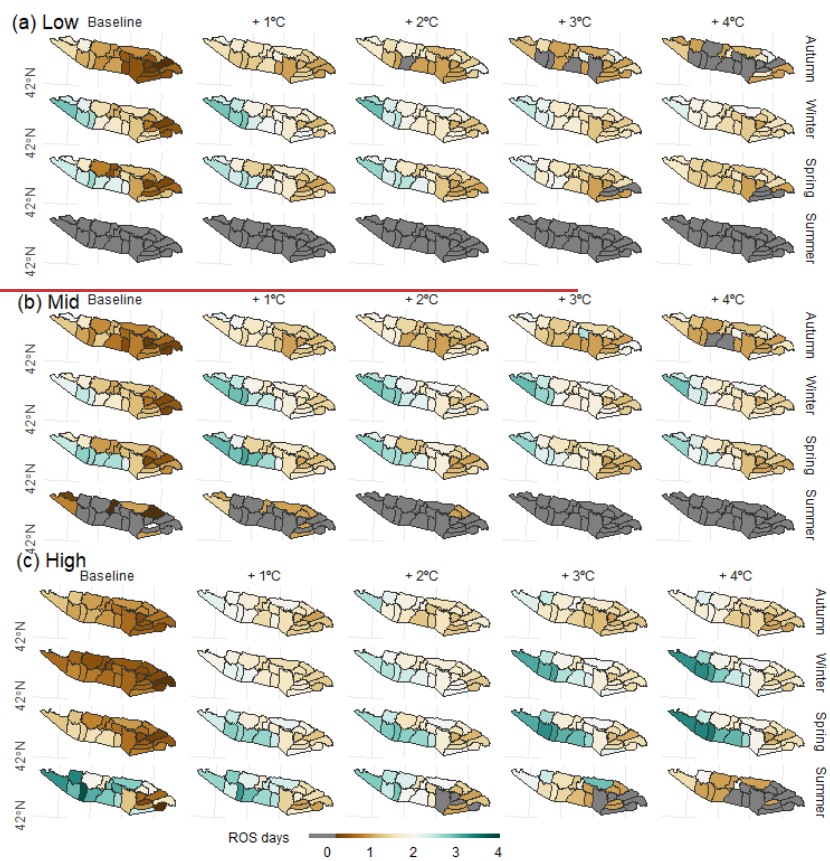


286

287

288 **Figure 43. ROS-#ROS frequency** for baseline climate period (1980-2019) and increments of temperature,
 289 grouped by months (x-axis), sector (rows) and elevation (columns).

290
291
292 ~~ROS frequency~~ response to warming vary depending on the month, increment of temperature, elevation,
293 and sector. ROS tends to disappear in October for ~~low-1500 m~~ elevations except in SW (Figure 4 and 53). The
294 highest increases are seen during the winter for increments temperature lower than 3°C, particularly in NE,
295 where ~~ROS frequency~~ increases 1 day per month over the baseline scenario for + 1°C. In ~~mid-1800 m~~
296 elevation, ~~ROS frequency~~ increases in all regions from November to February (around 1 day per month,
297 for + 1°C up to + 3°C). Similar increases are expected in NW and SW during the earliest months of spring and
298 for ~~low-1500 m~~ to moderate increments of temperature. The contrary is observed during the latest months of
299 spring in SW, where warming reduces ROS events. A slight ~~ROS frequency~~ increase is found during
300 spring for the rest of the sectors (Figure 4). ROS events in June are expected to disappear for temperature
301 increases higher than 1°C. Finally, ~~high-2400 m~~ elevation shows the largest ~~ROS frequency~~ variations
302 (around 1 day/month for + 1°C). Maximum ~~ROS frequency~~ increases (3 days/month) are found in SW
303 for more than + 3°C. ~~ROS frequency~~ progressively increases in March and April for all sectors but tends
304 to decrease in May (for + 3°C), June and July (for + 1°C).
305



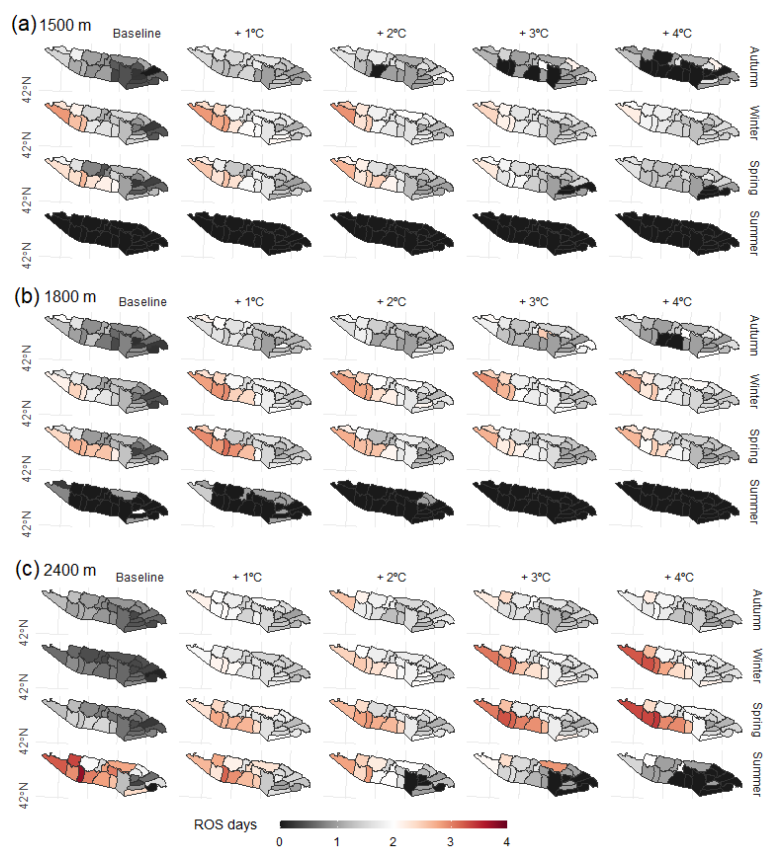


Figure 54. Average ROS frequency (days) for a season for (a) 1500 m, (b) 1800 m and (c) 2400 m elevation. Data are shown for the baseline climate period (1980-2019) and increment of temperature (left to right).

4.3 ROS rainfall amount

The spatial and temporal distribution of ROS rainfall amount is presented in Figure 65 and 76. The average ROS rainfall amount by year is 23, 28, 21, and 20 mm/day for SW, SE, NW, NE sectors, respectively. Similarly, the highest values in 1800 m elevation are found in SE (29 mm/day, respectively). SE sector experiences the highest ROS rainfall amount during autumn and summer (around 40 mm/day in 1500 m and 1800 m elevations). High 2400 m elevation maximum ROS rainfall amount values are however found in the western Pyrenees during the onset and offset snow season. Here, the largest ROS rainfall amount spatial and seasonal distribution ranges from SW (29 mm/day, autumn), NW (28 mm/day, summer), SE (24 mm/day, autumn) to NE (23 mm/day, autumn).

323

324

325

326

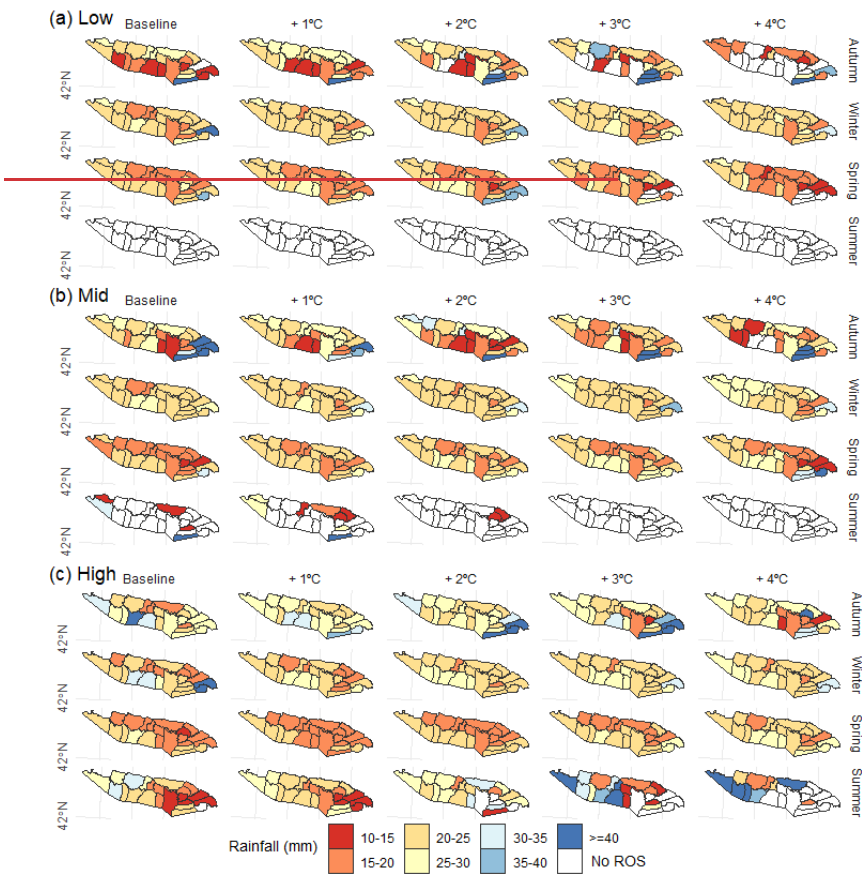
327

328

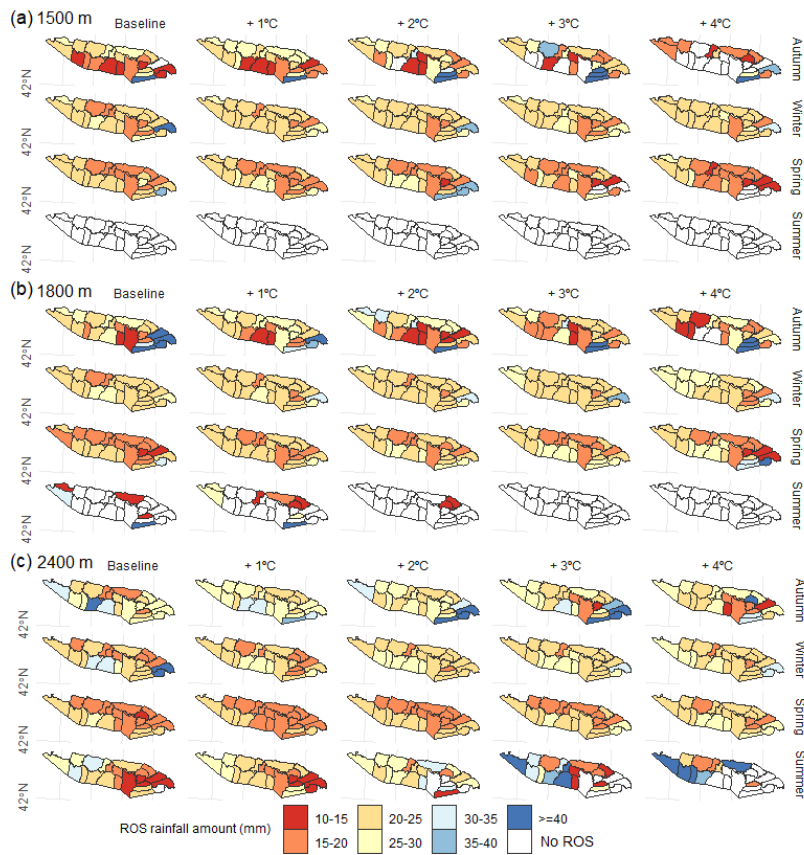


Figure 65. ROS rainfall amount (mm) temporal evolution for baseline climate (1980-2019) and

329 increment of warming (colors), grouped by elevation (columns) and sector (rows).
 330
 331 ~~ROS-rain~~ROS rainfall amount progressively increases due to warming (4%, 4%, and 5% per °C for low-, mid-,
 332 1800 m, and high- 2400 m elevations, respectively; Table S2). Small differences are found by elevation and
 333 sector. ~~Low- 1500 m~~ elevation ~~ROS-rain~~ROS rainfall amount increases until + 3°C, and generally decreases
 334 for + 4°C during the earliest (October to December) and latest (April and May) months of the snow season.
 335 Similar patterns are found in ~~mid- 1800 m~~ elevation. ~~ROS-rain~~ROS rainfall amount increases up to + 4°C,
 336 except in the SE sector for specific months (Figure 65). The latter sector shows also maximum ~~ROS-rain~~ROS
 337 rainfall amount values in autumn due to torrential rainfall. ~~High- 2400 m~~ elevation ~~ROS-rain~~ROS rainfall
 338 amount increase at a constant rate of around 5 % per °C. Yet, maximum increases are modeled in SW during
 339 summer, when ~~ROS-rain~~ROS rainfall amount almost doubles the baseline climate (+ 40% for + 4°C).
 340



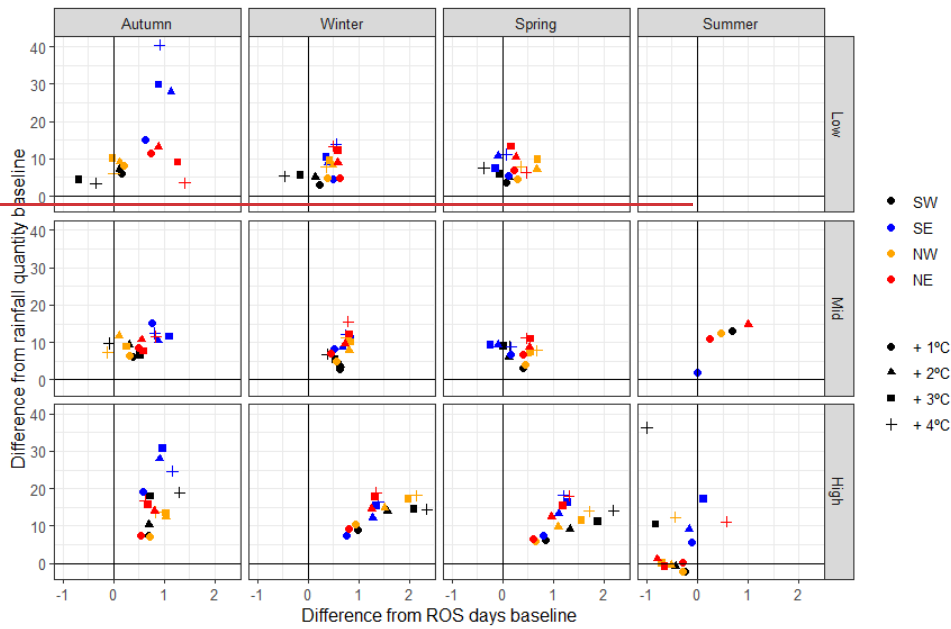
341



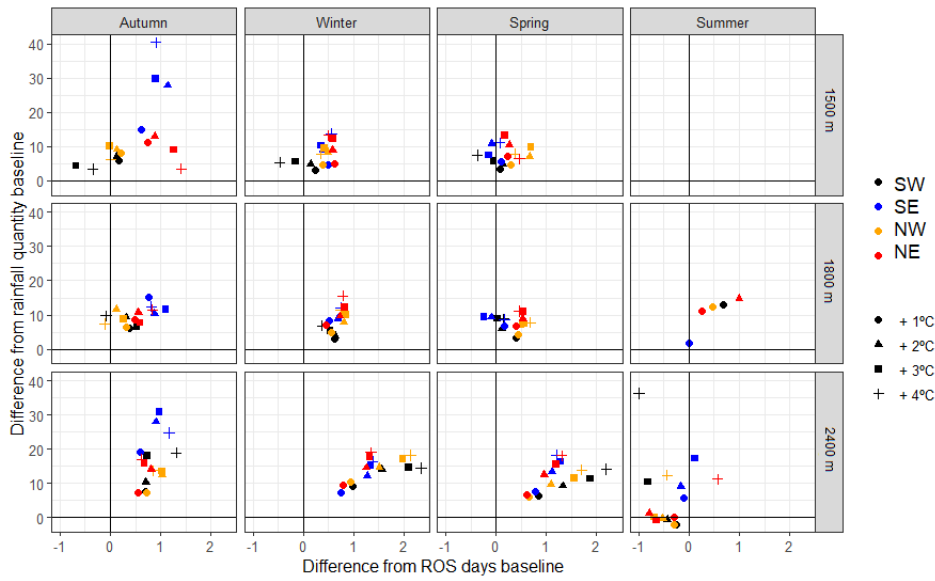
342
 343 **Figure 76.** Average ROS rainfall amount (mm) for a season for (a) 1500 m low, (b) mid- 1800 m
 344 and (c) high- 2400 m elevation. Data are shown for the baseline climate period (1980-2019) and increment of
 345 temperature (left to right).

346
 347 Data suggest that ROS exposure generally increases for all elevations and sectors during winter (except in SW
 348 for temperatures greater than 3°C). Nonetheless, remarkable spatial and seasonal differences are found. SE
 349 show the maximum values in autumn. On the contrary, small changes in frequency are detected in SW and
 350 NW, despite ROS rainfall amount is expected to increase (< 10mm/day). For the majority of sectors
 351 and elevations, ROS exposure generally increases in winter and spring. The minimum differences between
 352 sectors are detected in these seasons. In summer, ROS exposure tends to generally decrease for all elevations
 353 under severe warming due to snow cover depletion.
 354

355



356



357

358

359

360

361

Figure 87. Average ROS exposure. Points are obtained by a scatterplot between ~~ROS-rain~~ROS rainfall amount difference from baseline climate period (1980-2019) (y-axis) and ROS days difference from baseline climate (x-axis). Data is calculated by the average difference between (a) the baseline scenario (1980-2019) and (b) the different perturbed scenarios, only for the massifs where ~~ROS-fr~~ROS frequency exists on (a) and (b). Data are shown for each season (columns), elevation (rows), sector (color) and increment of temperature

(point shape).

4.4. ROS ablation

ROS ablation is presented at Figure 98 and 109. ROS ablation ranges from -10 cm/day in NW-high-2400 m elevation (summer) to -5 cm/day in NE-high-2400 m elevation (winter). ROS ablation nearly doubles the average daily snow ablation for all days on a season (Figure S56). Comparison with the reference baseline period reveals contrasting ROS ablation changes depending on the season, elevation and sector. Overall ROS ablation progressively increases due to warming in coldest zones and months of the season. The largest ROS ablation increments are detected in autumn and winter. For the former, ROS ablation increases at a generally constant rate in SW (11 %) NE (19 %) and NW (4 % per °C). For the latter, ROS ablation increases also in SW (11 %), NW (14 %) and NE (34 % per °C). In detail, maximum ROS ablation due to warming is found for mid-1800 m elevation during autumn (Figure 98). ROS ablation exhibit slow and no-changes in the warmest zone (SE), as well in the warmest months of the season, regardless the elevation band.



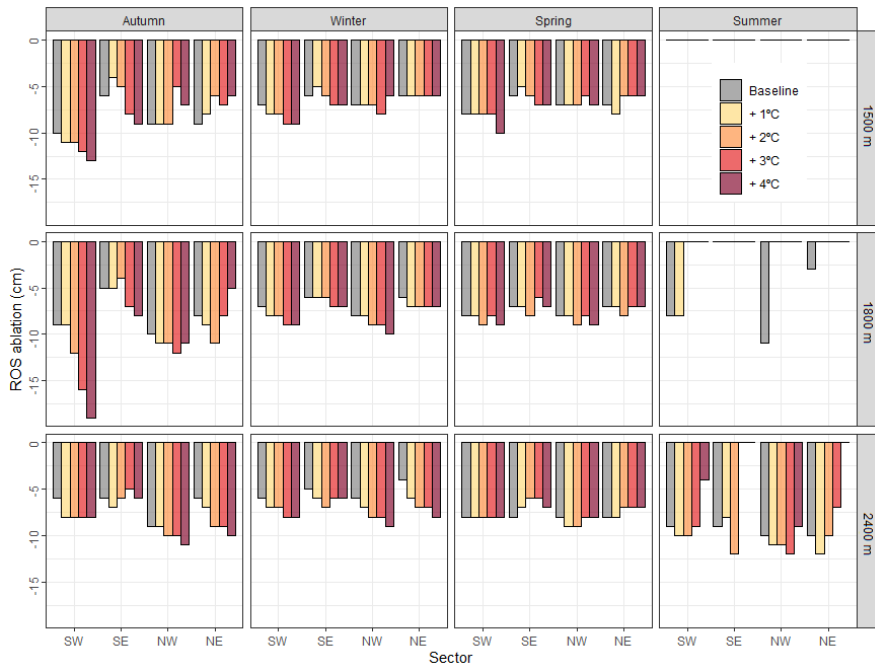
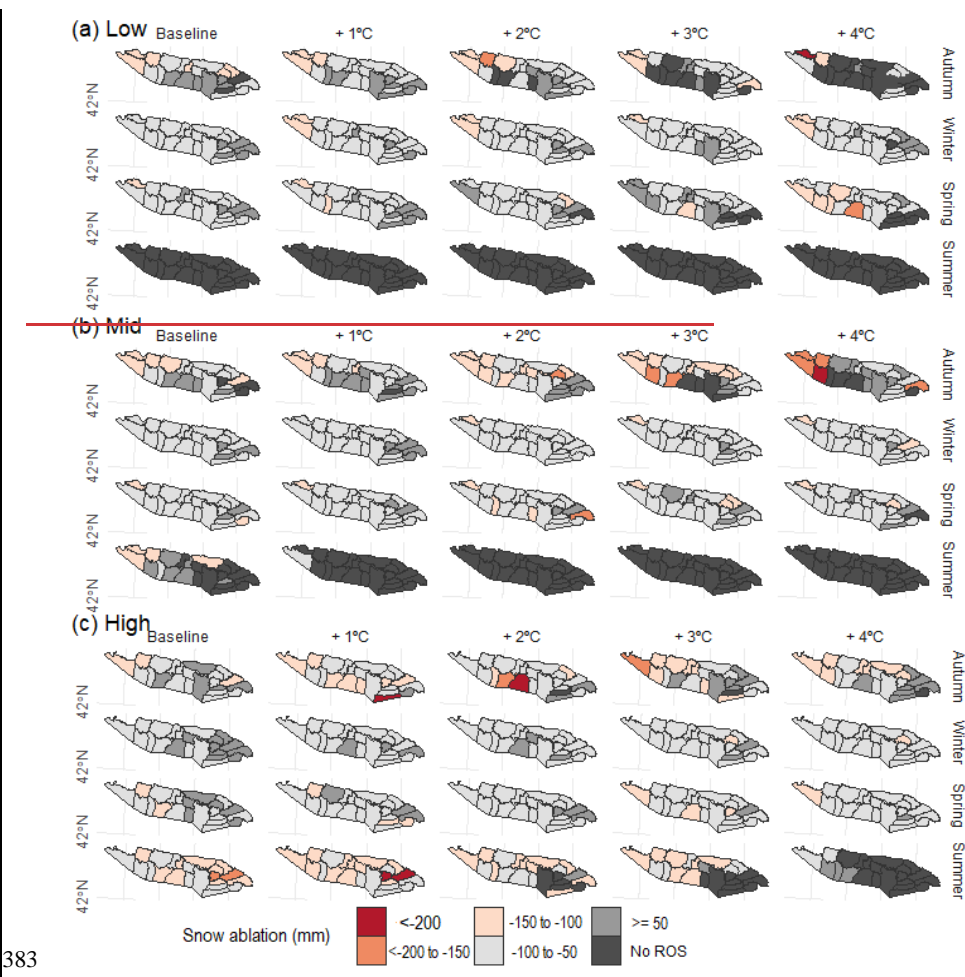


Figure 98. ROS ablation (y-axis) for baseline climate period (1980-2019) and increment of temperature (colors), sector (x-axis), season (columns) and elevation (rows).



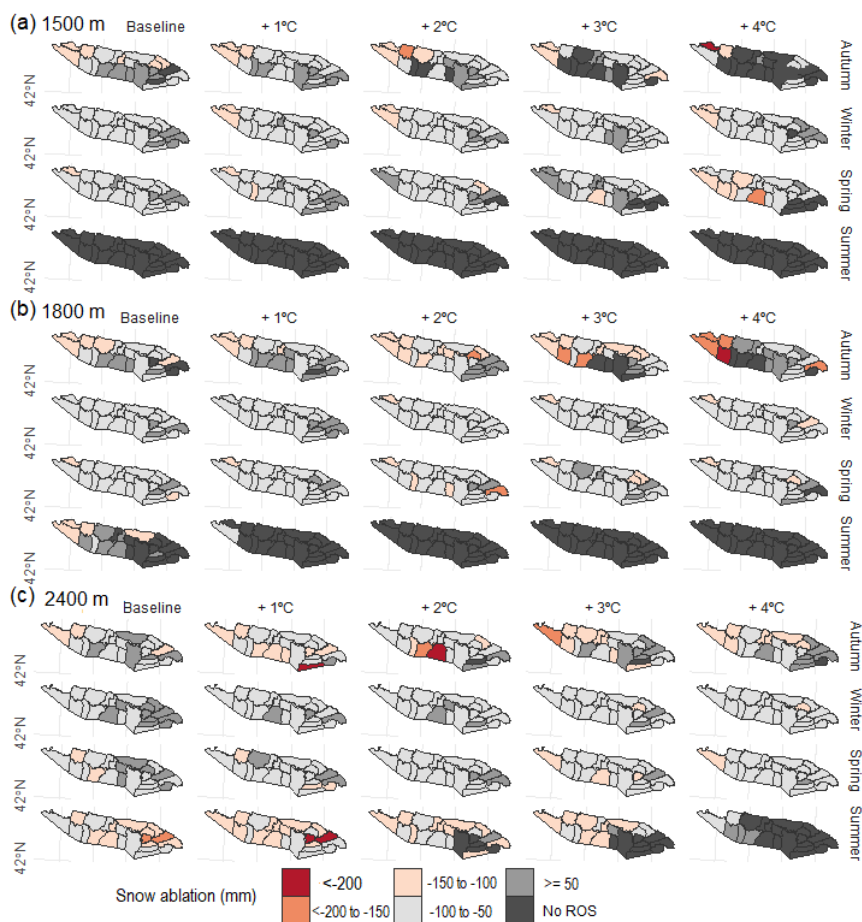


Figure 109. Average ROS ablation for a season for (a) 1500 m low, (b) mid-1800 m and (c) high-2400 m elevation. Data are shown for the baseline climate period (1980-2019) and increment of temperature (left to right).

Con formato: Fuente:

5 Discussion

The Pyrenees experienced a statistically significant positive temperature trend since the 1980s (ca. + 0.2 °C/decade) but no statistically significant precipitation trends are detected (OPCC, 2018) due to strong spatial (Vicente-Serrano et al., 2017), inter-annual and long-term variability of the latter (Peña-Angulo et al., 2021). Depending on the study period different snow trends were found. From ca. 1980 to 2010, non-statistically significant snow days and snow accumulation positive trends were generally detected at > 1000 m (Buisan et

al., 2016), 1800 m (Serrano-Notivol et al., 2018), and > 2000 m (Bonsoms et al., 2021a). Long-term trends (1957 to 2017), however, reveal statistically-significant snow depth decreases at 2100 m, but large variability depending on the sector and the snow indicator (López-Moreno et al., 2020). Climate projections for the end of the 21st century suggest an increase of temperature (> 3°C), together with ~~low- 1500 m~~ precipitation shifts (< 10%) from autumn to spring (Amblar-Francés et al., 2020). Within this climate context, ROS spatio-temporal patterns will likely change. In order to anticipate future scenarios, ROS sensitivity to warming was analyzed through three key indicators of frequency, rainfall intensity and snow ablation.

5.1 ROS spatial variability

The climatic setting of the Pyrenees as well as its relief configuration determines a remarkable spatial and temporal variability of ROS events. The contradiction between rainfall ratio increases and snowpack reductions, as well as the ~~high- 2400 m~~ spatial and monthly differences found, explain the complex ROS response to warming. HS decrease by 39 %, 37 % and 28 % per °C, for ~~1500 m~~, ~~low, mid- 1800 m~~ and ~~high- 2400 m~~ elevations, respectively. Similarly, Sf decreases by 29 %, 22 %, and 12 % per °C for ~~low-, 1500 m, 1800 m~~, ~~mid~~, and ~~high- 2400 m~~ elevations, respectively, providing evidence of an elevation-dependent snow sensitivity to temperature change. HS and Sf maximum reductions are reached for 1°C of warming, suggesting non-linear HS decreases, in accordance with previous snow sensitivity to climate change reported in central Pyrenees (López-Moreno et al., 2013). In detail, SW and NW annual ~~ROS-#ROS frequency~~ almost doubles (17 and 12 days/year, respectively) the one recorded in SE and NE (9 days/year, for both sectors). Maximum ~~ROS-#ROS frequency~~ for a season are found in SW and NW because of larger snow magnitudes in this sector (i.e., López-Moreno, 2005; López-Moreno et al, 2007; Navarro-Serrano et al., 2017; Bonsoms et al., 2021a). Thus, snow cover last longer until spring when minimum Sf values are found (Figure S1). This sector is the most exposed to SW and W air flows (negative NAO phases) (López-Moreno, 2005), which bring wet and mild conditions over the mountain range, leading to most ROS-related floods in the range (Morán-Tejeda et al., 2019). The generally ~~ROS-rainROS rainfall amount~~ increase reported in this work (independently of the increment of temperature and elevation) is explained by the Sf reduction expected for all sectors (Figure 32). Maximum ~~ROS-rainROS rainfall amount~~ is generally detected in spring (May), except in NE-~~high- 2400 m~~ elevation zones and SE (all elevations). In the latter sectors, ~~ROS-rainROS rainfall amount~~ tends to disappear in October under large (> 2°C) increments of temperature. The seasonal snow accumulation in NE and SE is lower-than-average due to the lower influence of Atlantic climate in these sectors of the range. Hence, large increments of warming decreases ~~ROS-#ROS frequency~~ due to snow cover depletion in early autumn and late spring (Figure S1). In addition, SE is closer to the 0°C due to higher-than-average sublimation, latent and radiative heat fluxes (Bonsoms et al., 2022*) and for this reason in this sector each increment of temperature has larger effects on the Sf, HS and ~~ROS-#ROS frequency~~ reduction (Figure 32). ~~High- 2400 m~~ elevation show the largest variation over the baseline climate as well as ROS exposure because of the larger snowpack magnitude and duration compared to ~~low- 1500 m~~ and ~~mid- 1800 m~~ areas. Thus, ~~high- 2400 m~~ elevation snow duration last until spring and summer, when the largest shift from snowfall to rainfall is found. On the other

hand, mid-1800 m elevation shows the maximum ~~ROS-rain~~ROS rainfall amount since the amount of moisture for condensation decreases while air masses increase height (Roe and Baker, 2006). Furthermore, the largest ~~ROS-rain~~ROS rainfall amount is detected in SE during autumn (Figure 76), because of the exposure of this region to Mediterranean low-pressure systems (negative WeMO phases), that usually trigger heavy rainfall events during this season (Lemus-Canovas et al., 2021).

5.2 ROS temporal evolution

Recent ROS trends in other mid-latitude areas are in accordance with ROS analysis presented here. Freudiger et al. (2013) analyzed the ROS trends (1950–2011 period) of the Rhine, Danube, Elbe, Weser, Oder, and Ems (Central Europe) basins. They found an overall ~~ROS-f~~ROS frequency increase during January and February (1990 to 2011 period), which is consistent with the ~~ROS-rain~~ROS rainfall amount and frequency increase detected in winter for the Pyrenees for all elevations and increment of temperature. Similarly, in Sitter River (NE Switzerland), a ~~ROS-f~~ROS frequency increase of around 40% (200%) at <1500 m (>2500 m) was detected between 1960 and 2015 (Beniston and Stoffel, 2016). During the last half of the 20th century, ~~ROS-f~~ROS frequency trends show an upward (downward) trend in high (low) elevation in western United-States (McCabe et al., 2007), as well as in southern British Columbia (Loukas et al., 2002) and at catchment scale in Oregon (United-States) (Surfleet and Tullos, 2013). Same ~~ROS-f~~ROS frequency increases (decreases) has been detected from 1980 to 2010 in Norwegian high (low) elevated mountain zones (Pall et al., 2019). However, in contradiction with our results and previous studies, winter Northern-Hemisphere ~~ROS-f~~ROS frequency trends (1979-2014 period) show no-clear trends (Cohen et al., 2015).

Results exposed in this work provide more evidence of ~~ROS-f~~ROS frequency increases in high-elevation zones, as it has been suggested by climate projections and ROS sensitivity to temperature studies. ROS show an elevation-dependent pattern that was previously reported in the Swiss Alps (Morán-Tejeda et al., 2016). In Sitter River (NE Switzerland), an increase of 2 to 4 °C over the 1960 to 2015 period results in an increase of the ~~ROS-f~~ROS frequency by around 50% at > 2500 m (Beniston and Stoffel, 2016). Likewise, 21st century high-emission scenarios (RCP8.5), suggest increases in ~~ROS-f~~ROS frequency and intensity in Gletsch (Switzerland) high-elevation area; however, on climate projections for ROS definitions that include snow melting (Musselman et al., 2018), natural climate variability contributes to a large extend (70 %) of ROS variability (Schirmer et al., 2022). Li et al. (2019) analyzed the future ~~ROS-f~~ROS frequency in the conterminous United-States and detected a nonlinear trend ROS due to warming, which is consistent with the different ~~ROS-rain~~ROS rainfall amount and frequency responses depending on the increment of temperature detected in our work. Climate projections for the mid-end of the 21th century projected positive ~~ROS-f~~ROS frequency and rainfall trends in Western United-States and Canada (il Jeong and Sushama, 2018). Similarly, ~~ROS-f~~ROS frequency will likely decrease (increase) in the warmest months of the season in low (high) elevation areas of western United-States (Musselman et al., 2018). The same is projected Norwegian mountains (Mooney and Li, 2021). López-Moreno et al. (2021) analyzed 40 worldwide basins ROS sensitivity to

473 warming. In their study they found a decrease of ROS events in warm mountain areas. However, they detected
474 ~~ROS-#ROS frequency~~ increases in cold-climate mountains where large snow accumulation is found despite
475 warming. In accordance with our results, they identified large seasonal differences and ~~ROS-#ROS frequency~~
476 decreases in Mediterranean mountains due to snow cover depletion in the last months of the snow season.

478 5.3 ROS ablation

479
480 Warming increases ROS ablation from autumn to winter on deep snowpacks and in the coldest sectors of the
481 range, due to higher energy for snow ablation and closer 0°C isotherm conditions in a warmer than baseline
482 climate. Nevertheless, data show ~~low- 1500 m~~ or decreases in ROS ablation in SE and spring, since the
483 snowpack is already near to the isothermal conditions. These results go in line with results modelled for cold
484 and warm Pyrenean sites (López-Moreno et al., 2013) as well as for different Northern-Hemisphere sites
485 (Essery et al., 2020). ROS ablation indicator is also indirectly affected by the HS magnitude decreases (30 %
486 per °C; Figure 32), and therefore lower ROS ablation is directly affected by lower HS magnitudes. Previous
487 literature pointed out that warming have counter-intuitive effects on snow ablation patterns. Higher than
488 average temperatures advance the peak HS date on average 5 days per °C in ~~mid- 1800 m~~ and ~~high- 2400 m~~
489 elevations (Bonsoms et al., 2022b), triggering earlier snow ablation onsets, and therefore lower solar radiation
490 fluxes (López-Moreno et al., 2013; Lundquist et al., 2013; Pomeroy et al., 2015; Musselman et al., 2017a;
491 Sanmiguel-Valladolid et al., 2022), as well as earlier snow depletion before the maximum advection of heat
492 fluxes into the snowpack (spring) (Bonsoms et al., 2022a). Slower snow melt rates in a warmer climate have
493 been detected in Western United-States (Musselman et al., 2017), as well as the entire Northern-Hemisphere
494 (Wu et al., 2018). ~~Low- 1500 m~~ or inexistent changes in snow ablation on warm and marginal snowpacks has
495 been previously detected in the central Pyrenees (López-Moreno et al., 2013), in forest and open areas
496 (Sanmiguel-Valladolid et al., 2022), in the entire range (Bonsoms et al., 2022b), and other Iberian Peninsula
497 Mountain ranges outside the Pyrenees (Alonso-González et al., 2020a).

498 ROS ablation is larger than the average snow ablation during a snow ablation day (Figure S6) due to higher
499 SEB positive fluxes. Several works analyzed SEB changes on ROS events, and different SEB contributions
500 has been found depending on the geographical area (Mazurkiewicz et al., 2008; Garvelmann et al., 2014b;
501 Würzer et al., 2016; Corripio and López-Moreno, 2017; Li et al., 2019), ranging from net radiation in Pacific
502 North West (Mazurkiewicz et al., 2008) to Lwin and turbulent heat fluxes in conterminous United-States
503 mountain areas (Li et al., 2019) or the Swiss Alps (e.g., Würzer et al., 2016). In general, studies in mid-latitude
504 mountain ranges have shown that turbulent heat fluxes contribute between 60 and 90 % of the energy available
505 for snow ablation during ROS days (e.g., Marks et al., 1998; Garvelmann et al. 2014; Corripio and López-
506 Moreno, 2017). In the central Pyrenees (> 2000 m) the meteorological analysis of a ROS event reveals that
507 ROS ablation is larger than a normal ablation day because of the large advection of Lwin and especially
508 sensible heat fluxes (Corripio and López-Moreno, 2017). Lwin increases due to the high cloud cover and warm

air, as it is frequently observed during ROS episodes (Moore and Owens, 1984). Further works should analyze the SEB controls during ROS events within the entire mountain range, as well as the ROS hydrological responses to climate warming.

512

513 5.4 ROS socio-environmental impacts and hazards

Temperature-induced changes in the seasonal snowpack and during ROS days suggest several hydrological shifts including, but not limited to, earlier peak flows on the season (Surfleet and Tullos, 2013), rapid streamflow peaks during high precipitation events in frozen soils (Shanley and Chalmers, 1999), faster soil moisture depletion and lower river discharges in spring due to earlier snow melt in the season (Stewart, 2009). The shortening of the snow season due to warming reported in this work will potentially alter alpine phenological patterns (i.e., Wipf and Rixen, 2010) and expand forest cover (Szczypta et al., 2015). Although vegetation branches intercepts a large amount of snowfall, intermediate and high vegetation shields short-wave radiation, reduces snow wind-transport and turbulent heat fluxes (López-Moreno and Latron, 2008; Sanmiguel-Valellado et al., 2022). Snow-forest interactions, their sensitivity to climate change as well as the ROS hydrological response within a changing landscape is far from understood across the range and should be the base of forecoming works.

525

The higher ROS exposure (Figure 87) will likely imply an increase of ROS-related hazards and impacts in the mountain ecosystem. Heavy ~~ROS-rain~~ROS rainfall amount changes snow metamorphism on saturated snowpacks and leads to high-speed water percolation (Singh et al., 1997). The subsequent water refreezing changes the snowpack conditions and creates an ice-layer in the snowpack that can reach the surface (Rennert et al., 2009). ROS can cause plant damage (Bjerke et al., 2017) and the ice encapsulation of vegetation in tundra ecosystems can trigger severe wildlife impacts, such as vertebrate herbivores starvation (Hansen et al 2013), reindeer population mortality (Kohler and Aanes, 2004) and higher competition between species (Hansen et al 2014). Nevertheless, any study to the date analyzed ROS-related impacts in flora and fauna across Southern-European mountains. Snow albedo decay due positive heat fluxes and rainfall in ROS events (Corripio and López-Moreno, 2017), lead to faster snow ablation even on the next days (e.g., Singh et al. 1997). The combination of changes in internal snowpack processes, larger ~~ROS-rain~~ROS rainfall amount, and more energy to ablate snow during spring could enhance snow runoff, especially during warm and wet snowpack conditions (Würzer et al., 2016). In snow-dominated regions ROS can lead to a specific type of avalanching (Conway and Raymond, 1993) and floods (Surfleet and Tullos, 2013). The latter are the most environmental damaging risk in Spain (Llasat et al., 2014) and around 50% of the flood in the Iberian Peninsula are due to ROS events (Morán-Tejeda et al., 2019). More than half of the historical (1940 to 2012) flood events in the Ésera river catchment (central Pyrenees) occurred during spring (Serrano-Notivoli et al., 2017), which coincides with the snow ablation season. ROS floods have also economic impacts. For instance, a ROS flood

544 event that occurred on 13th June of 2013 in the Garonne River (Val d'Aran, central Pyrenees) cost
545 approximately 20 million of euros to the public insurance (Llasat et al., 2014).

546

547 5.5 Limitations

548

549 This study evaluates the sensitivity of ROS responses to climate change, enabling a better understanding of
550 the non-linear ROS spatiotemporal variations in different sectors and elevations of the Pyrenees. Instead of
551 presenting diverse outputs from climate model ensembles (López-Moreno et al., 2010), we provide ROS
552 sensitivity values per 1°C, making them comparable to other regions and seasons. The temperature and
553 precipitation change values used in this sensitivity analysis are based on established climate projections for the
554 region (Amblar-Francés et al., 2020). However, precipitation projections in the Pyrenees exhibit high
555 uncertainties among different models, GHGs emission scenarios, and temporal periods (López-Moreno et al.,
556 2008).

557

558 The SAFRAN meteorological system used in this work relies on a topographical spatial division and exhibit
559 and accuracy of around 1 °C in Ta and around 20 mm in the monthly cumulative precipitation (Vernay et al.,
560 2022). Precipitation phase partitioning methods are subject to uncertainties under close-to-isothermal
561 conditions (Harder et al., 2010). Hydrological models are also subject to errors in the snowpack prediction
562 (Essery, 2015). However, the FSM2 is a multiphysics snowpack model that has been validated previously in
563 the Pyrenees (Bonsoms et al., 2023) and compared against different snowpack models (Krinner et al., 2018),
564 providing evidence of its robustness.

565

566

567 **6 Conclusions**

568 The expected decreases in Sf and HS due to climate warming will likely change ROS spatio-temporal patterns
569 across the Pyrenees. Therefore, a better understanding of ROS is required. This work analyzed the ROS
570 sensitivity to warming by forcing a physically based snow model with perturbed reanalysis climate data (1980-
571 2019 period) for 1500 m low, mid- 1800 m and high- 2400 m elevation areas of the Pyrenees. ROS ~~delta-~~
572 changesensitivity to temperature and precipitation is evaluated by frequency, rainfall intensity and snow
573 ablation during ROS days.

574 During the baseline climate period, annual ~~ROS-#~~ROS frequency totals on average 10, 12 and 10 day/season
575 for 1500 m low, mid- 1800 m and high- 2400 m elevations. Higher-than-average annual ~~ROS-#~~ROS frequency
576 are found in mid- 1800 m elevation SW (17 days/year) and NW (12 days/year), which contrast with the
577 minimums detected in SE (9 days/year). The different spatial and seasonal ROS response to warming suggest
578 that contrasting and shifting trends could be expected in the future. Overall ~~ROS-#~~ROS frequency decreases
579 during summer in high- 2400 m elevation for > 1°C. When temperature is progressively increased the greatest

580 ~~ROS frequency~~ increases are found for SW ~~high- 2400 m~~ elevation (around 1 day/month for + 1°C).
581 ~~ROS frequency~~ is highly sensitive to warming in the snow onset and offset months, when
582 counterintuitive factors play a key role. On the one hand, maximum Sf decreases are modeled for spring,
583 leading to rainfall increases; on the other hand, warming depletes the snowpack in the warmest and snow driest
584 sectors of the range. Consequently, data suggest a general ~~ROS frequency~~ decrease for the majority of
585 the SE massifs, where the snowpack is near the isothermal conditions in the baseline climate period. Yet, during
586 spring, the highest ~~ROS frequency~~ increases are detected in SW and NW, since these sectors are less
587 exposed to radiative and turbulent heat fluxes and record higher-than-average seasonal snow accumulations.

588 ~~ROS rainfall amount~~ generally increases due to warming, independently of the sector and elevation,
589 being limited by the number of ROS days. The largest and constant increments are observed in spring, when
590 ~~ROS rainfall amount~~ increases at a rate of 7, 6 and 3 % per °C for ~~low-, mid- 1800 m~~ and high,
591 respectively. ~~ROS rainfall amount~~ increases are explained by Sf reductions, which decrease at a rate
592 of 29 %, 22 %, and 12 % per °C for ~~low-, 1500 m, 1800 m mid-, and high- 2400 m~~ elevations, respectively. ~~ROS~~
593 ~~rainfall amount~~ maximum values are detected in SE (28 mm/day), especially in ~~mid- 1800 m~~ elevation
594 during autumn (45 mm/day), since this sector is exposed to subtropical Mediterranean flows.

595 Finally, ROS ablation shows contrasting patterns depending on the season, sector and elevation. Generally,
596 ROS ablation increases in cold snowpacks, such as those modeled in ~~high- 2400 m~~ elevation and during cold
597 seasons (autumn and winter). Here, ROS ablation follows a constant ablation rate of around + 10% per °C, due
598 to higher-than-average positive sensible and LWin heat fluxes. However, in SE and ~~low- 1500 m~~ elevations,
599 where marginal and isothermal snowpacks are found, no changes or decreases in ROS ablation are detected
600 due to snowpack magnitude reductions in a warmer climate. Results demonstrate the high snow sensitivity to
601 climate within a mid-latitude mountain range, and suggest significant changes with regards to water resources
602 management. Relevant implications in the ecosystem and socio-economic activities associated with snow
603 cover are anticipated ~~d.d.~~

604
605
606

607 Data availability

608 FSM2 is an open access snow model (Essery, 2015) provided at <https://github.com/RichardEssery/FSM2> (last
609 access 15 January 2023). SAFRAN climate dataset (Vernay et al., 2022) is available by AERIS at
610 <https://www.aeris-data.fr/landing-page/?uuid=865730e8-edeb-4c6b-ae58-80f95166509b#v2020.2> (last access
611 16 December 2022). Data of this work is available upon request by the first author (josephbonsoms5@ub.edu).

612 Author contribution

613 J.B., J.I.L.M., and E.A.G. designed the work. J.B. analyzed the data and wrote the manuscript. J.B., J.I.L.M.,
614 E.A.G., C.D.B., and M.O. provided feedback and edited the manuscript. J.I.L.M., M.O. supervised the project
615 and acquired funding.

616 **Competing interests**

617 The authors declare that they have no conflict of interest.

618 **Acknowledgements**

619 This work frames within the research topics examined by the research group “Antarctic, Artic, Alpine
620 Environments-ANTALP” (2017-SGR-1102) funded by the Government of Catalonia, HIDROIBERNIEVE
621 (CGL2017-82216-R) and MARGISNOW (PID2021-124220OB-100), from the Spanish Ministry of Science,
622 Innovation and Universities. JB is supported by a pre-doctoral University Professor FPI grant (PRE2021-
623 097046) funded by the Spanish Ministry of Science, Innovation and Universities.

624 625 **References**

- 626
627 Alonso-González, E., Aalstad, K., Baba, M. W., Revuelto, J., López-Moreno, J. I., Fiddes, J., et al. MuSA: The
628 Multiscale Snow Data Assimilation System (v1.0). Geoscientific Model Development Discussions, 1–43.
629 <https://doi.org/10.5194/gmd-2022-137>, 2022.
- 630
631 Alonso-González, E., López-Moreno, J.I., Navarro-Serrano, F., Sanmiguel-Valladolid, A., Aznárez-Balta, M.,
632 Revuelto, J., and Ceballos, A.: Snowpack Sensitivity to Temperature, Precipitation, and Solar Radiation
633 Variability over an Elevational Gradient in the Iberian Mountains, Atmos. Res., 243, 104973 <https://doi.org/10.1016/j.atmosres.2020.104973>, 2020a.
- 634
635
636 Alonso-González, E., López-Moreno, J.I., Navarro-Serrano, F., Sanmiguel-Valladolid, A., Revuelto, J.,
637 Domínguez-Castro, F., and Ceballos, A.: Snow climatology for the mountains in the Iberian Peninsula using
638 satellite imagery and simulations with dynamically downscaled reanalysis data, International Journal of
639 Climatology, 40(1), 477–491, <https://doi.org/10.1002/joc.6223>, 2019.
- 640
641 Alonso-González, E., López-Moreno, J. I., Navarro-Serrano, F. M., and Revuelto, J.: Impact of North Atlantic
642 Oscillation on the snowpack in Iberian Peninsula mountains, Water (Switzerland), 12,
643 <https://doi.org/10.3390/w12010105>, 2020b.
- 644
645 Amblar-Francés, M. P., Ramos-Calzado, P., Sanchis-Lladó, J., Hernanz-Lázaro, A., Peral-García, M. C.,
646 Navascués, B., Domínguez-Alonso, M., Pastor-Saavedra, M. A., and Rodríguez-Camino, E.: High resolution
647 climate change projections for the Pyrenees region, in: Advances in Science and Research, 191–208,
648 <https://doi.org/10.5194/asr-17-191-2020>, 2020.
- 649
650 Barnett, T.P., Adam, J.C., and Lettenmaier, D.P., Potential impacts of a warming climate on water availability
651 in snow-dominated regions. Nature. <https://doi.org/10.1038/nature04141>, 2005.
- 652
653 Bartsch, A., Kumpula, T., Forbes, B. C., and Stammer, F.: Detection of snow surface thawing and refreezing
654 in the Eurasian arctic with QuikSCAT: Implications for reindeer herding, Ecological Applications, 20, 2346–
655 2358, <https://doi.org/10.1890/09-1927.1>, 2010.

654 Beniston, M. and Stoffel, M.: Rain-on-snow events, floods and climate change in the Alps: Events may increase
655 with warming up to 4 °C and decrease thereafter, *Science of the Total Environment*, 571, 228–236,
656 <https://doi.org/10.1016/j.scitotenv.2016.07.146>, 2016.

657 Beniston, M., Farinotti, D., Stoffel, M., Andreassen, L. M., Coppola, E., Eckert, N., Fantini, A., Giacona, F.,
658 Hauck, C., Huss, M., Huwald, H., Lehning, M., López-Moreno, J. I., Magnusson, J., Marty, C., Morán-Tejeda,
659 E., Morin, S., Naaim, M., Provenzale, A., Rabatel, A., Six, D., Stötter, J., Strasser, U., Terzago, S., and Vincent,
660 C.: The European mountain cryosphere: A review of its current state, trends, and future challenges,
661 <https://doi.org/10.5194/tc-12-759-2018>, 2018.

662 Bieniek, P. A., Bhatt, U. S., Walsh, J. E., Lader, R., Griffith, B., Roach, J. K., and Thoman, R. L.: Assessment
663 of Alaska rain-on-snow events using dynamical downscaling, *J Appl Meteorol Climatol*, 57, 1847–1863,
664 <https://doi.org/10.1175/JAMC-D-17-0276.1>, 2018.

665 Bintanja, R. and Andry, O.: Towards a rain-dominated Arctic, *Nat Clim Chang*, 7, 263–267,
666 <https://doi.org/10.1038/nclimate3240>, 2017.

667 Bonsoms, J., Franch, F. S., and Oliva, M.: Snowfall and snow cover evolution in the eastern pre-pyrenees (Ne
668 iberian peninsula), *Geographical Research Letters*, 47, 291–307, <https://doi.org/10.18172/cig.4879>, 2021a.

669 Bonsoms, J., González, S., Prohom, M., Esteban, P., Salvador-Franch, F., López-Moreno, J. I., and Oliva, M.:
670 Spatio-temporal patterns of snow in the Catalan Pyrenees (NE Iberia), *International Journal of Climatology*,
671 41, 5676–5697, <https://doi.org/10.1002/joc.7147>, 2021b.

672 Bonsoms, J., López-Moreno, J. I., González, S., and Oliva, M.: Increase of the energy available for snow
673 ablation in the Pyrenees (1959–2020) and its relation to atmospheric circulation, *Atmos Res*, 275,
674 <https://doi.org/10.1016/j.atmosres.2022.106228>, 2022a.

675 Bonsoms, J., López-Moreno, J. I., and Alonso-González, E.: Snow sensitivity to temperature and precipitation
676 change during compound cold-hot and wet-dry seasons in the Pyrenees, *The Cryosphere*, 17, 1307–1326,
677 <https://doi.org/10.5194/tc-17-1307-2023>, 2023.

678 Buisan, S.T., López-Moreno, J.I., Sanz, M.A. and Korchendorfer, J. Impact of weather type variability on
679 winter precipitation, temperature and annual snowpack in the Spanish Pyrenees. *Climate Research*, 69, 79–92.
680 <https://doi.org/10.3354/cr01391>, 2016.

681 Bjerke JW, Treharne R, Vikhamar-Schuler D, Karlsen S R, Ravolainen V, Bokhorst S, Phoenix G K, Bochenek
682 Z and Tømmervik H 2017 Understanding the drivers of extensive plant damage in boreal and Arctic
683 ecosystems: insights from field surveys in the aftermath of damage *Sci. Total Environ.* 599 1965–76.

684 Ceron, J. P., Tanguy, G., Franchistéguy, L., Martin, E., Regimbeau, F., and Vidal, J. P.: Hydrological seasonal
685 forecast over France: Feasibility and prospects, *Atmospheric Science Letters*, 11, 78–82,
686 <https://doi.org/10.1002/asl.256>, 2010.

687 Cohen, J., Ye, H., and Jones, J.: Trends and variability in rain-on-snow events, *Geophys Res Lett*, 42, 7115–
688 7122, <https://doi.org/10.1002/2015GL065320>, 2015.

689 Collados-Lara, A. J., Pulido-Velazquez, D., Pardo-Igúzquiza, E., and Alonso-González, E.: Estimation of the
690 spatio-temporal dynamic of snow water equivalent at mountain range scale under data scarcity, *Science of the*
691 *Total Environment*, 741, <https://doi.org/10.1016/j.scitotenv.2020.140485>, 2020.

692 Conway, H. and Raymond, C. F.: Snow stability during rain, *Journal of Glaciology*, 39, 635–642,

693 <https://doi.org/10.3189/s0022143000016531>, 1993.

694 Corripio, J. G. and López-Moreno, J. I.: Analysis and predictability of the hydrological response of mountain
695 catchments to heavy rain on snow events: A case study in the Spanish Pyrenees, *Hydrology*, 4,
696 <https://doi.org/10.3390/hydrology4020020>, 2017.

697 Crawford, A. D., Alley, K. E., Cooke, A. M., and Serreze, M. C.: Synoptic Climatology of Rain-on-Snow
698 Events in Alaska, <https://doi.org/10.1175/MWR-D-19>, 2020.

699 Deschamps-Berger, C., Cluzet, B., Dumont, M., Lafaysse, M., Berthier, E., Fanise, P., and Gascoin, S.:
700 Improving the Spatial Distribution of Snow Cover Simulations by Assimilation of Satellite Stereoscopic
701 Imagery, *Water Resour. Res.*, 58, e2021WR030271, <https://doi.org/10.1029/2021WR030271>, 2022.
702

703 Del Barrio, G., Creus, J., and Puigdefabregas, J.: Thermal Seasonality of the High Mountain Belts of the
704 Pyrenees, *Mt. Res. Dev.*, 10, 227–233, 1990.

705 Devers, A., Vidal, J. P., Lauvernet, C., and Vannier, O.: FYRE Climate: A high-resolution reanalysis of daily
706 precipitation and temperature in France from 1871 to 2012, *Climate of the Past*, 17, 1857–1879,
707 <https://doi.org/10.5194/cp-17-1857-2021>, 2021.

708 Durand, Y., Giraud, G., Brun, E., Mérindol, L., and Martin, E.: A computer-based system simulating snowpack
709 structures as a tool for regional avalanche forecasting, *Journal of Glaciology*, 45, 469–484,
710 <https://doi.org/10.3189/s0022143000001337>, 1999.

711 Durand, Y., Laternser, M., Giraud, G., Etchevers, P., Lesaffre, B., and Mérindol, L.: Reanalysis of 44 yr of
712 climate in the French Alps (1958–2002): Methodology, model validation, climatology, and trends for air
713 temperature and precipitation, *J Appl Meteorol Climatol*, 48, 429–449,
714 <https://doi.org/10.1175/2008JAMC1808.1>, 2009.

715 Essery, R.: A factorial snowpack model (FSM 1.0), *Geosci Model Dev*, 8, 3867–3876,
716 <https://doi.org/10.5194/gmd-8-3867-2015>, 2015.
717

718 Essery, R., Kim, H., Wang, L., Bartlett, P., Boone, A., Brutel-Vuilmet, C., Burke, E., Cuntz, M., Decharme,
719 B., Dutra, E., Fang, X., Gusev, Y., Hagemann, S., Haverd, V., Kontu, A., Krinner, G., Lafaysse, M., Lejeune,
720 Y., Marke, T., Marks, D., Marty, C., Menard, C. B., Nasonova, O., Nitta, T., Pomeroy, J., Schädler, G.,
721 Semenov, V., Smirnova, T., Swenson, S., Turkov, D., Wever, N., and Yuan, H.: Snow cover duration trends
722 observed at sites and predicted by multiple models, *Cryosphere*, 14, 4687–4698, [https://doi.org/10.5194/tc-](https://doi.org/10.5194/tc-14-4687-2020)
723 14-4687-2020, 2020.

724 Freudiger, D., Kohn, I., Stahl, K., and Weiler, M.: Large-scale analysis of changing frequencies of rain-on-
725 snow events with flood-generation potential, *Hydrol Earth Syst Sci*, 18, 2695–2709,
726 <https://doi.org/10.5194/hess-18-2695-2014>, 2014.

727 García-Ruiz, J. M., López-Moreno, J. I., Vicente-Serrano, S. M., Lasanta-Martínez, T. and Beguería, S.
728 Mediterranean water resources in a global change scenario, *Earth Sci. Rev.*, 105(3–4), 121–139,
729 <https://doi.org/10.1016/j.earscirev.2011.01.006>, 2011.

730 Garvelmann, J., Pohl, S., and Weiler, M.: Variability of observed energy fluxes during rain-on-snow and clear
731 sky snowmelt in a midlatitude mountain environment, *J Hydrometeorol*, 15, 1220–1237,
732 <https://doi.org/10.1175/JHM-D-13-0187.1>, 2014.

733 Günther, D., Marke, T., Essery, R., and Strasser, U.: Uncertainties in Snowpack Simulations—Assessing the

734 Impact of Model Structure, Parameter Choice, and Forcing Data Error on Point-Scale Energy Balance Snow
735 Model Performance, *Water Resour Res*, 55, 2779–2800, <https://doi.org/10.1029/2018WR023403>, 2019.

736 Habets, F., Boone, A., Champeaux, J. L., Etchevers, P., Franchistéguy, L., Leblois, E., Ledoux, E., le Moigne,
737 P., Martin, E., Morel, S., Noilhan, J., Seguí, P. Q., Rousset-Regimbeau, F., and Viennot, P.: The SAFRAN-
738 ISBA-MODCOU hydrometeorological model applied over France, *Journal of Geophysical Research*
739 *Atmospheres*, 113, <https://doi.org/10.1029/2007JD008548>, 2008.

740 Hansen, B.B., Grotan, V., Aanes, R., et al., 2013. Climate events synchronize the dynamics of a resident
741 vertebrate community in the High Arctic. *Science* 339, 313–315.

742 Hansen, B.B., Isaksen, K., Benestad, R.E., et al., 2014. Warmer and wetter winters: characteristics and
743 implications of an extreme weather event in the High Arctic. *Environ. Res. Lett.* 9, 114021.

744 [Harder, P. and Pomeroy, J.: Estimating precipitation phase using a psychrometric energy balance method,](#)
745 [Hydrological Processes](#), 27(13), 1901–1914. <https://doi.org/10.1002/hyp.9799>, 2013

746 Immerzeel, W. W., Lutz, A. F., Andrade, M., Bahl, A., Biemans, H., Bolch, T., Hyde, S., Brumby, S., Davies,
747 B. J., Elmore, A. C., Emmer, A., Feng, M., Fernández, A., Haritashya, U., Kargel, J. S., Koppes, M.,
748 Kraaijenbrink, P. D. A., Kulkarni, A. v., Mayewski, P. A., Nepal, S., Pacheco, P., Painter, T. H., Pellicciotti, F.,
749 Rajaram, H., Rupper, S., Sinisalo, A., Shrestha, A. B., Viviroli, D., Wada, Y., Xiao, C., Yao, T., and Baillie, J.
750 E. M.: Importance and vulnerability of the world's water towers, *Nature*, 577, 364–369,
751 <https://doi.org/10.1038/s41586-019-1822-y>, 2020.

752 IPCC: High Mountain Areas, in: *The Ocean and Cryosphere in a Changing Climate*, Cambridge University
753 Press, 131–202, <https://doi.org/10.1017/9781009157964.004>, 2022.

754 Jennings, K. S., Winchell, T. S., Livneh, B., and Molotch, N. P.: Spatial variation of the rain-snow temperature
755 threshold across the Northern Hemisphere, *Nat Commun*, 9, <https://doi.org/10.1038/s41467-018-03629-7>,
756 2018.

757 il Jeong, D. and Sushama, L.: Rain-on-snow events over North America based on two Canadian regional
758 climate models, *Clim Dyn*, 50, 303–316, <https://doi.org/10.1007/s00382-017-3609-x>, 2018.

759 Kohler, J. and Aanes, R.: Effect of winter snow and ground-icing on a Svalbard reindeer population: Results
760 of a simple snowpack model, in: *Arctic, Antarctic, and Alpine Research*, 333–341,
761 [https://doi.org/10.1657/1523-0430\(2004\)036\[0333:EOWSAG\]2.0.CO;2](https://doi.org/10.1657/1523-0430(2004)036[0333:EOWSAG]2.0.CO;2), 2004.

762 [Krinner, G., Derksen, C., Essery, R., Flanner, M., Hagemann, S., Clark, M., Hall, A., Rott, H., Brutel-](#)
763 [Vuilmet, C., Kim, H., Ménard, C. B., Mudryk, L., Thackeray, C., Wang, L., Arduini, G., Balsamo, G.,](#)
764 [Bartlett, P., Boike, J., Boone, A., Chérut, F., Colin, J., Cuntz, M., Dai, Y., Decharme, B., Derry, J.,](#)
765 [Ducharne, A., Dutra, E., Fang, X., Fierz, C., Ghattas, J., Gusev, Y., Haverd, V., Kontu, A., Lafaysse, M.,](#)
766 [Law, R., Lawrence, D., Li, W., Marke, T., Marks, D., Ménégoz, M., Nasonova, O., Nitta, T., Niwano, M.,](#)
767 [Pomeroy, J., Raleigh, M. S., Schaedler, G., Semenov, V., Smirnova, T. G., Stacke, T., Strasser, U.,](#)
768 [Svenson, S., Turkov, D., Wang, T., Wever, N., Yuan, H., Zhou, W., and Zhu, D.: ESM-SnowMIP: assessing](#)
769 [snow models and quantifying snow-related climate feedbacks, Geosci. Model Dev.](#), 11, 5027–5049,
770 <https://doi.org/10.5194/gmd-11-5027-2018>, 2018.

771 Lemus-Canovas, M., Lopez-Bustins, J. A., Trapero, L., and Martin-Vide, J.: Combining circulation weather
772 types and daily precipitation modelling to derive climatic precipitation regions in the Pyrenees, *Atmos Res*,
773 220, 181–193, <https://doi.org/10.1016/j.atmosres.2019.01.018>, 2019.

Con formato: Fuente: (Predeterminada) Times New Roman

774 Lemus-Canovas, M., Lopez-Bustins, J. A., Martín-Vide, J., Halifa-Marin, A., Insua-Costa, D., Martinez-
775 Artigas, J., Trapero, L., Serrano-Notivoli, R., and Cuadrat, J. M.: Characterisation of extreme precipitation
776 events in the Pyrenees: From the local to the synoptic scale, *Atmosphere (Basel)*, 12,
777 <https://doi.org/10.3390/atmos12060665>, 2021.

778 Li, D., Lettenmaier, D. P., Margulis, S. A., and Andreadis, K.: The Role of Rain-on-Snow in Flooding Over
779 the Conterminous United States, *Water Resour Res*, 55, 8492–8513, <https://doi.org/10.1029/2019WR024950>,
780 2019.

781 Llasat, M. C., Marcos, R., Llasat-Botija, M., Gilabert, J., Turco, M., and Quintana-Seguí, P.: Flash flood
782 evolution in North-Western Mediterranean, *Atmos Res*, 149, 230–243,
783 <https://doi.org/10.1016/j.atmosres.2014.05.024>, 2014.

784 López-Moreno, J. I.: Recent variations of snowpack depth in the central Spanish Pyrenees, *Arct Antarct Alp*
785 *Res*, 37, 253–260, [https://doi.org/10.1657/1523-0430\(2005\)037\[0253:RVOSDI\]2.0.CO;2](https://doi.org/10.1657/1523-0430(2005)037[0253:RVOSDI]2.0.CO;2), 2005.

786 [López-Moreno, J.I., Govette, S., and Beniston, M.: Climate change prediction over complex areas: spatial](#)
787 [variability of uncertainties and predictions over the Pyrenees from a set of regional climate models.](#)
788 [International Journal of Climatology](#), 28, 1535–1550. <https://doi.org/10.1002/joc.1645>, 2008.

789 López-Moreno, J. I., Pomeroy, J. W., Revuelto, J., and Vicente-Serrano, S. M.: Response of snow processes to
790 climate change: Spatial variability in a small basin in the Spanish Pyrenees, *Hydrol Process*, 27, 2637–2650,
791 <https://doi.org/10.1002/hyp.9408>, 2013.

792 López-Moreno, J. I., Pomeroy, J. W., Morán-Tejeda, E., Revuelto, J., Navarro-Serrano, F. M., Vidaller, I., and
793 Alonso-González, E.: Changes in the frequency of global high mountain rain-on-snow events due to climate
794 warming, *Environmental Research Letters*, 16, <https://doi.org/10.1088/1748-9326/ac0dde>, 2021.

795 López-Moreno, J.I., Soubeyroux, J.M., Gascoin, S., Alonso-González, E., Durán-Gómez, N., Lafaysse, M.,
796 Vernay, M., Carmagnola, C. and Morin, S. Long-term trends (1958–2017) in snow cover duration and depth
797 in the Pyrenees. *International Journal of Climatology*, 40, 1–15. <https://doi.org/10.1002/joc.6571>, 2020.

798 López-Moreno, J.I., and Vicente-Serrano, S.M.: Atmospheric circulation influence on the interannual
799 variability of snowpack in the Spanish Pyrenees during the second half of the twentieth century, *Nord. Hydrol.*,
800 38 (1), 38–44, <https://doi.org/10.2166/nh.2007.030>, 2007.

801 López-Moreno, J.I., and Latron, J., 2008. Spatial heterogeneity in snow water equivalent induced by forest
802 canopy in a mixed beech-fir stand in the Pyrenees. *Ann. Glaciol.* 49 (1), 83–90,
803 <https://doi.org/10.3189/172756408787814951>, 2008.

804 Loukas, A., Vasiliades, L., and Dalezios, N. R.: Potential climate change impacts on flood producing
805 mechanisms in southern British Columbia, Canada using the CGCMA1 simulation results, *J. Hydrol.*, 259,
806 163–188, [https://doi.org/10.1016/S0022-1694\(01\)00580-7](https://doi.org/10.1016/S0022-1694(01)00580-7), 2002.

807 Lundquist, J. D., Dickerson-Lange, S. E., Lutz, J. A., and Cristea, N. C.: Lower forest density enhances snow
808 retention in regions with warmer winters: A global framework developed from plot-scale observations and
809 modeling, *Water Resour Res*, 49, 6356–6370, <https://doi.org/10.1002/wrcr.20504>, 2013.

810 Lynn, E., Cuthbertson, A., He, M., Vasquez, J. P., Anderson, M. L., Coombe, P., Abatzoglou, J. T., and Hatchett,
811 B. J.: Technical note: Precipitation-phase partitioning at landscape scales to regional scales, *Hydrol Earth Syst*
812 *Sci*, 24, 5317–5328, <https://doi.org/10.5194/hess-24-5317-2020>, 2020.

813 Mاتیو, M., Crespi, A., Bertoldi, G., Carmagnola, C.M., Marty, C., Morin, S., Schöner, W., Cat Berro, D.,
814 Chiogna, G., De Gregorio, L., Kotlarski, S., Majone, B., Resch, G., Terzago, S., Valt, M., Beozzo, W.,
815 Cianfarra, P., Gouttevin, I., Marcolini, G., Notarnicola, C., Petitta, M., Scherrer, S.C., Strasser, U., Winkler,
816 M., Zebisch, M., Cicogna, A., Cremonini, R., Debernardi, A., Faletto, M., Gaddo, M., Giovannini, L., Mercalli,
817 L., Soubeyroux, J.-M., Susnik, A., Trenti, A., Urbani, S., Weilguni, V. Observed snow depth trends in the
818 European Alps 1971 to 2019. *Cryosphere*, 1–50. <https://doi.org/10.5194/tc-2020-289>, 2020.

819 Marks, D., Link, T., Winstral, A., and Garen, D.: Simulating snowmelt processes during rain-on-snow over a
820 semi-arid mountain basin, 1992.

821 Marty, C., Schlögl, S., Bavay, M., and Lehning, M.: How much can we save? Impact of different emission
822 scenarios on future snow cover in the Alps, *Cryosphere*, 11, 517–529, <https://doi.org/10.5194/tc-11-517-2017>,
823 2017.

824 Mazurkiewicz, A. B., Callery, D. G., and McDonnell, J. J.: Assessing the controls of the snow energy balance
825 and water available for runoff in a rain-on-snow environment, *J Hydrol (Amst)*, 354, 1–14,
826 <https://doi.org/10.1016/j.jhydrol.2007.12.027>, 2008.

827 Mazzotti, G., Essery, R., Webster, C., Malle, J., and Jonas, T.: Process-Level Evaluation of a Hyper-Resolution
828 Forest Snow Model Using Distributed Multisensor Observations, *Water Resour Res*, 56,
829 <https://doi.org/10.1029/2020WR027572>, 2020.

830 McCabe, G. J., Clark, M. P., and Hay, L. E.: Rain-on-snow events in the Western United-States,
831 <https://doi.org/10.1175/BAMS-88-3-319>, 2007.

832 Mooney, P. A. and Li, L.: Near future changes to rain-on-snow events in Norway, *Environmental Research*
833 *Letters*, 16, <https://doi.org/10.1088/1748-9326/abfdeb>, 2021.

834 Morán-Tejeda, E., López-Moreno, J. I., Stoffel, M., and Beniston, M.: Rain-on-snow events in Switzerland:
835 Recent observations and projections for the 21st century, *Clim Res*, 71, 111–125,
836 <https://doi.org/10.3354/cr01435>, 2016.

837 Morán-Tejeda, E., Fassnacht, S. R., Lorenzo-Lacruz, J., López-Moreno, J. I., García, C., Alonso-González, E.,
838 and Collados-Lara, A. J.: Hydro-meteorological characterization of major floods in Spanish mountain rivers,
839 *Water (Switzerland)*, 11, <https://doi.org/10.3390/W11122641>, 2019.

840 Morin, S., Horton, S., Techel, F., Bavay, M., Coléou, C., Fierz, C., Gobiet, A., Hagenmuller, P., Lafaysse, M.,
841 Ližar, M., Mitterer, C., Monti, F., Müller, K., Olefs, M., Snook, J. S., van Herwijnen, A., and Vionnet, V.:
842 Application of physical snowpack models in support of operational avalanche hazard forecasting: A status
843 report on current implementations and prospects for the future,
844 <https://doi.org/10.1016/j.coldregions.2019.102910>, 2020.

845 Musselman, K. N., Clark, M. P., Liu, C., Ikeda, K., and Rasmussen, R.: Slower snowmelt in a warmer world,
846 *Nat Clim Chang*, 7, 214–219, <https://doi.org/10.1038/nclimate3225>, 2017a.

847 Musselman, K. N., Keitholotch, N. P., Mar, N., and Mgulis, S. A.: Snowmelt response to simulated warming
848 across a large elevation gradient, southern sierra Nevada, California, *Cryosphere*, 11, 2847–2866,
849 <https://doi.org/10.5194/tc-11-2847-2017>, 2017b.

850 Musselman, K. N., Lehner, F., Ikeda, K., Clark, M. P., Prein, A. F., Liu, C., Barlage, M., and Rasmussen, R.:
851 Projected increases and shifts in rain-on-snow flood risk over western North America,

852 <https://doi.org/10.1038/s41558-018-0236-4>, 2018.

853 Navarro-Serrano, F. and López-Moreno, J. I.: Análisis espacio-temporal de los eventos de nevadas en el pirineo
854 Español y su relación con la circulación atmosférica, Cuadernos de Investigacion Geografica, 43, 233–254,
855 <https://doi.org/10.18172/cig.3042>, 2017.

856 Ohba, M. and Kawase, H.: Rain-on-Snow events in Japan as projected by a large ensemble of regional climate
857 simulations, Clim Dyn, 55, 2785–2800, <https://doi.org/10.1007/s00382-020-05419-8>, 2020.

858

859 OPCC-CTP. Climate change in the Pyrenees: Impacts, vulnerabilities and adaptation bases of knowledge for
860 the future climate change adaptation strategy in the Pyrenees. 2018. 147. Jaca, Spain.
861 <https://www.opccctp.org/sites/default/files/editor/opcc-informe-en-paginas.pdf>. (last acces December 25,
862 2022)

863 Pall, P., Tallaksen, L. M., and Stordal, F.: A Climatology of Rain-on-Snow Events for Norway,
864 <https://doi.org/10.1175/JCLI-D-18>, 2019.

865 Pepin, N. C., Arnone, E., Gobiet, A., Haslinger, K., Kotlarski, S., Notarnicola, C., Palazzi, E., Seibert, P.,
866 Serafin, S., Schöner, W., Terzago, S., Thornton, J. M., Vuille, M., and Adler, C.: Climate Changes and Their
867 Elevational Patterns in the Mountains of the World, <https://doi.org/10.1029/2020RG000730>, 2022.

868 Peña-Angulo, D., Vicente-Serrano, S., Domínguez-Castro, F., Murphy, C., Reig, F., Trambly, Y., Trigo, R.,
869 Luna, M.Y., Turco, M., Noguera, I., Aznarez-Balta, M., Garcia-Herrera, R., Tomas-Burguera, M. and Kenawy,
870 A. Long-term precipitation in Southwestern Europe reveals no clear trend attributable to anthropogenic
871 forcing. Environmental Research Letters, 15, 094070 <https://doi.org/10.1088/1748-9326/ab9c4f>, 2020.

872 ~~Pons, M., López-Moreno, J., Rosas-Casals, M., and Jover, E.: The vulnerability of Pyrenean ski resorts to~~
873 ~~climate-induced changes in the snowpack, Clim.Change, 131, 591–605, [https://doi.org/10.1007/s10584-015-](https://doi.org/10.1007/s10584-015-1400-8)~~
874 ~~[1400-8](https://doi.org/10.1007/s10584-015-1400-8), 2015.~~

875 Pomeroy, J. W., Fang, X., and Rasouli, K.: Sensitivity of snow processes to warming in the Canadian Rockies,
876 2015.

877 Pomeroy, J. W., Fang, X., and Marks, D. G.: The cold rain-on-snow event of June 2013 in the Canadian Rockies
878 — characteristics and diagnosis, Hydrol Process, 30, 2899–2914, <https://doi.org/10.1002/hyp.10905>, 2016.

879 ~~Quintana Seguí, P., le Moigne, P., Durand, Y., Martin, E., Habets, F., Baillon, M., Canellas, C., Franchisteguy,~~
880 ~~L., and Morel, S.: Analysis of near surface atmospheric variables: Validation of the SAFRAN analysis over~~
881 ~~France, J Appl Meteorol Climatol, 47, 92–107, <https://doi.org/10.1175/2007JAMC1636.1>, 2008.~~

882 ~~Quintana Seguí, P., Turco, M., Herrera, S., and Miguez Macho, G.: Validation of a new SAFRAN based~~
883 ~~gridded precipitation product for Spain and comparisons to Spain02 and ERA-Interim, Hydrol Earth Syst Sci,~~
884 ~~21, 2187–2201, <https://doi.org/10.5194/hess-21-2187-2017>, 2017.~~

885 Rasouli, K., Pomeroy, J. W., and Whitfield, P. H.: Hydrological responses of headwater basins to monthly
886 perturbed climate in the North American Cordillera, J Hydrometeorol, 20, 863–882,
887 <https://doi.org/10.1175/JHM-D-18-0166.1>, 2019.

888 Rennert, K. J., Roe, G., Putkonen, J., and Bitz, C. M.: Soil thermal and ecological impacts of rain on snow
889 events in the circumpolar arctic, J Clim, 22, 2302–2315, <https://doi.org/10.1175/2008JCLI2117.1>, 2009.

890 Réveillet, M., Dumont, M., Gascoin, S., Lafaysse, M., Nabat, P., Ribes, A., Nheili, R., Tuzet, F., Ménégoz, M.,

891 Morin, S., Picard, G., and Ginoux, P.: Black carbon and dust alter the response of mountain snow cover under
 892 climate change, *Nat Commun*, 13, <https://doi.org/10.1038/s41467-022-32501-y>, 2022.

893 Revuelto, J., Lecourt, G., Lafaysse, M., Zin, I., Charrois, L., Vionnet, V., Dumont, M., Rabatel, A., Six, D.,
 894 Condom, T., Morin, S., Viani, A., and Sirguey, P.: Multi-criteria evaluation of snowpack simulations in
 895 complex alpine terrain using satellite and in situ observations, *Remote Sens (Basel)*, 10,
 896 <https://doi.org/10.3390/rs10081171>, 2018.

897 Roe, G. H. and Baker, M. B.: *Microphysical and Geometrical Controls on the Pattern of Orographic*
 898 *Precipitation*, 2006.

899 Sanmiguel-Valladolid, A., McPhee, J., Esmeralda Ojeda Carreño, P., Morán-Tejeda, E., Julio Camarero, J., and
 900 López-Moreno, J. I.: Sensitivity of forest–snow interactions to climate forcing: Local variability in a Pyrenean
 901 valley, *J Hydrol (Amst)*, 605, <https://doi.org/10.1016/j.jhydrol.2021.127311>, 2022.

902

903 Schirmer, M., Winstral, A., Jonas, T., Burlando, P., and Peleg, N.: Natural climate variability is an important
 904 aspect of future projections of snow water resources and rain-on-snow events, *Cryosphere*, 16, 3469–3488,
 905 <https://doi.org/10.5194/tc-16-3469-2022>, 2022.

906 Schöner, W., Koch, R., Matulla, C., Marty, C., and Tilg, A. M.: Spatio-temporal patterns of snow depth within
 907 the Swiss-Austrian Alps for the past half century (1961 to 2012) and linkages to climate change, *International*
 908 *Journal of Climatology*, 39, 1589–1603, <https://doi.org/10.1002/joc.5902>, 2019.

909 Serrano-Notivol, R., Buisan, S.T., Abad-Pérez, L.M., Sierra-Álvarez, E., Rodríguez-Ballesteros, C., López-
 910 Moreno, J.I. and Cuadrat, J.M. Tendencias recientes en precipitación, temperatura y nieve de alta montaña en
 911 los Pirineos (Refugio de Góriz, Huesca). In: *El clima: aire, agua, tierra y fuego*. Madrid, Spain: Asociación
 912 Española de Climatología y Ministerio para la Transición Ecológica – Agencia Estatal de Meteorología, pp.
 913 267, 1060–280, 2018.

914 Serrano-Notivol, R., Mora, D., Ollero, A., Sánchez-Fabre, M., Sanz, P., and Saz, M.: Floodplain occupation
 915 and flooding in the central Pyrenees, *Cuadernos de Investigacion Geografica*, 43, 309–328,
 916 <https://doi.org/10.18172/cig.3057>, 2017.

917 Serreze, M. C., Gustafson, J., Barrett, A. P., Druckenmiller, M. L., Fox, S., Voveris, J., Stroeve, J., Sheffield,
 918 B., Forbes, B. C., Rasmus, S., Laptander, R., Brook, M., Brubaker, M., Temte, J., McCrystall, M. R., and
 919 Bartsch, A.: Arctic rain on snow events: Bridging observations to understand environmental and livelihood
 920 impacts, *Environmental Research Letters*, 16, <https://doi.org/10.1088/1748-9326/ac269b>, 2021.

921 Shanley, J. B. and Chalmers, A.: The effect of frozen soil on snowmelt runoff at Sleepers River, Vermont 1999.

922 Singh, P., Spitzbart, G., Hübl, H., and Weinmeister, H. W.: Hydrological response of snowpack under rain-on-
 923 snow events: a field study, *Journal of Hydrology*, 1–20 pp., 1997.

924 Smyth, E. J., Raleigh, M. S., and Small, E. E. (2020). Improving SWE estimation with data assimilation: The
 925 influence of snow depth observation timing and uncertainty. *Water Resources Research*, 56, e2019WR026853.
 926 <https://doi.org/10.1029/2019WR026853>

927 Spandre, P., François, H., Verfaillie, D., Lafaysse, M., Déqué, M., Eckert, N., George, E., and Morin, S.:
 928 Climate controls on snow reliability in French Alps ski resorts, *Sci Rep*, 9, [https://doi.org/10.1038/s41598-](https://doi.org/10.1038/s41598-019-44068-8)
 929 [019-44068-8](https://doi.org/10.1038/s41598-019-44068-8), 2019.

930 Stewart, I. T.: Changes in snowpack and snowmelt runoff for key mountain regions,
931 <https://doi.org/10.1002/hyp.7128>, 2009.

932 Surfleet, C. G. and Tullos, D.: Variability in effect of climate change on rain-on-snow peak flow events in a
933 temperate climate, *J Hydrol (Amst)*, 479, 24–34, <https://doi.org/10.1016/j.jhydrol.2012.11.021>, 2013.

934 Szczypta, C., Gascoin, S., Houet, T., Hagolle, O., Dejoux, J.-F., Vigneau, C., and Fanise, P.: Impact of climate
935 and land cover changes on snow cover in a small Pyrenean catchment, *J. Hydrol.*, 521, 84–99,
936 [doi:10.1016/j.jhydrol.2014.11.060](https://doi.org/10.1016/j.jhydrol.2014.11.060), 2015.

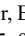
937 Verfaillie, D., Lafaysse, M., Déqué, M., Eckert, N., Lejeune, Y., and Morin, S.: Multi-component ensembles
938 of future meteorological and natural snow conditions for 1500 m altitude in the Chartreuse mountain range,
939 *Northern French Alps, Cryosphere*, 12, 1249–1271, <https://doi.org/10.5194/tc-12-1249-2018>, 2018.

940 Vernay, M., Lafaysse, M., Monteiro, D., Hagenmuller, P., Nheili, R., Samacoïts, R., Verfaillie, D., and Morin,
941 S.: The S2M meteorological and snow cover reanalysis over the French mountainous areas: description and
942 evaluation (1958-2021), *Earth Syst Sci Data*, 14, 1707–1733, <https://doi.org/10.5194/essd-14-1707-2022>,
943 2022.

944 Vicente-Serrano, S.M., Rodríguez-Camino, E., Domínguez-Castro, F., El Kenawy, A., Azorín-Molina, C. An
945 updated review on recent trends in observational surface atmospheric variables and their extremes over Spain.
946 *Cuadernos de Investigación Geográfica (Geographical Research Letters)* 43 (1), 209-232.
947 <https://doi.org/10.18172/cig.3134>, 2017.

948 Vidaller, I., Revuelto, J., Izagirre, E., Rojas-Heredia, F., Alonso-González, E., Gascoin, S., René, P., Berthier,
949 E., Rico, I., Moreno, A., Serrano, E., Serreta, A., López-Moreno, J.I. Toward an ice-free mountain range:
950 Demise of Pyrenean glaciers during 2011–2020. *J. Geophys. Res. Lett.* 48, e2021GL094339
951 <https://doi.org/10.1029/2021GL094339>, 2021.

952 Viviroli, D., Archer, D. R., Buytaert, W., Fowler, H. J., Greenwood, G. B., Hamlet, A. F., Huang, Y.,
953 Koboltschnig, G., Litaor, M. I., López-Moreno, J. I., Lorentz, S., Schädler, B., Schreier, H., Schwaiger, K.,
954 Vuille, M., and Woods, R.: Climate change and mountain water resources: Overview and recommendations
955 for research, management and policy, *Hydrol Earth Syst Sci*, 15, 471–504, [https://doi.org/10.5194/hess-15-](https://doi.org/10.5194/hess-15-471-2011)
956 471-2011, 2011.

957 Westermann, S., Boike, J., Langer, M., Schuler, T. , and Etzelmüller, B.: Modeling the impact of wintertime
958 rain events on the thermal regime of permafrost, *Cryosphere*, 5, 945–959, [https://doi.org/10.5194/tc-5-945-](https://doi.org/10.5194/tc-5-945-2011)
959 2011, 2011.

960 Wipf, S. and Rixen, C.: A review of snow manipulation experiments in Arctic and alpine tundra ecosystems,
961 <https://doi.org/10.1111/j.1751-8369.2010.00153.x>, 2010.

962 Wu, X., Che, T., Li, X., Wang, N., and Yang, X.: Slower Snowmelt in Spring Along With Climate Warming
963 Across the Northern Hemisphere, *Geophys Res Lett*, 45, 12,331-12,339,
964 <https://doi.org/10.1029/2018GL079511>, 2018.

965 Würzer, S., Jonas, T., Wever, N., and Lehning, M.: Influence of initial snowpack properties on runoff formation
966 during rain-on-snow events, *J Hydrometeorol*, 17, 1801–1815, <https://doi.org/10.1175/JHM-D-15-0181.1>,
967 2016.

968